A Thesis for the Degree of Master

Design, Control and VR-Navigation of a 6-DOF Gait Rehabilitation Robot with Upper- and Lower-Limb Connections

by

Bondhan Novandy

GYEONGSANG NATIONAL UNIVERSITY

Department of Mechanical & Aerospace Engineering

2009

Design, Control and VR-Navigation of a 6-DOF Gait Rehabilitation Robot with Upper- and Lower-Limb Connections

A Dissertation submitted to the Faculty of the Graduate School
of the Gyeongsang National University

by Bondhan Novandy

In partial fulfillment of the requirements
for the degree
of Master of Engineering

February, 2009

Prof. Jungwon Yoon, Dissertation Supervisor

Approved by committees of the Graduate School
of Gyeongsang National University in partial fulfillment
of the requirements for the degree of Master of Engineering

Dissertation Committee: Jungwon Yoon

Chairman

Sujin Kim

Sungkwan Kim

(Name and signature)

Date: 2009 . 01. 15.

Department of Mechanical & Aerospace Engineering
GRADUATE SCHOOL
GYEONGSANG NATIONAL UNIVERSITY

Table of Contents

List of Figures

List of Tables

ABSTRACT

Design, Control and VR-Navigation of a 6-DOF Gait Rehabilitation Robot with Upper- and Lower-Limb Connections

Bondhan Novandy
Department of Mechanical and Aerospace Engineering
Graduate School, Gyeongsang National University
Directed by
Professor Jungwon Yoon

Recently, several gait rehabilitation robots have been developed along with the advances of the understanding in rehabilitative mechanisms. One of the desirable objectives is that the patient should be allowed to influence the motion of the robot such as walking faster or slower according to his intentions. Also, long duration and repetitive training make the training become tedious and may reduce the rehabilitation outcome.

This thesis presents the development, control and VR-navigation of a 6-DOF gait rehabilitation robot which allows walking velocity update on various terrain types in virtual environment (VE) through upper- and lower-limb connections. The robot is composed of an upper-limb device, a sliding device, two footpad devices, and a partial body support system. The footpad device on the sliding device generates 3-DOF spatial motions on the sagittal plane for each foot.

This allows the generation of various terrain types for diverse walking training. The upper-limb device allows users to swing their arms naturally through the use of a simple pendulum link with a passive prismatic joint.

Synchronized gait patterns for this robot are designed to represent a normal gait with upper- and lower-limb connections. To permit patients to walk at will, this robot allows walking velocity updates for various terrain types by estimating the interaction torques between the human and the upper-limb device, and synchronizing the lower-limb device with the upper-limb device. In addition, the subject is able to navigate in VEs by generating turning commands with switches located in the handles of the upper-limb device.

Experimental results with a healthy subject show that the user can update the walking velocity on level ground, slopes, and stairs through upper- and lower-limb connections. In addition, the user could navigate in the VEs with walking velocity updates and turning input command allowing various rehabilitation training modes.

초록

상반신과 하반신에 대한 6자유도를 가진 재활 로봇의 VR 네비게이션 구현과 설계 그리고 제어

노반디 본드한
경상대학교 기계항공공학부 기계설계학과
지도 교수: 윤정원

오늘날, 우리는 주변에서 재활 메커니즘에 대한 전문가들에 의해 장애인들을 위한 재활 로봇이 개발 되고 있다는 것을 종종 접한다. 그러나 환자의 재활을 위해서 반복적이고 긴 훈련은 자칫 환자에게 지루함을 주고 재활 훈련의 성과도 감소 시킬 수도 있다. 이 논문에 소개된 로봇의 주요 기능 중의 하나는 환자가 빨리 걷고 싶거나 늦게 걷고 싶은 의도를 로봇이 반영할 수 있다는 것이다.

이 논문은 6-자유도를 가진 걸음 재활 로봇의 VR-네비게이션에 대해서 설명할 것이다. 이 로봇은 인간이 걸을 때 사지의 움직임을 통해서 가상환경 속의 여러 지형 때문에 일어나는 걸음걸이의 속력 변화가 가능하게 설계 되었다. 이 재활 로봇은 팔과 다리를 움직이는 부분과, 걸음을 흉내내기 위한 미끄럼 기능을 하는 부분, 발판 부분, 몸을 부분적으로 잡아주는 부분으로 구성되어 있다.

미끄럼 부분 위에 있는 발판은 각 발판의 시상(矢狀)면을 기준으로 3-자유도를 부여한다. 이러한 메카니즘을 통해 다양한 걸음 훈련을 위해서 다양한 지형을 구현할 수 있다. 사지를 움직여주는 부분에서 진자처럼

움직이는 간단한 장치를 통해 사용자의 자연스러운 팔의 움직임을 구현할 수 있다.

로봇이 환자의 걸음을 유도하는 모양은 우리가 평소 걸을 때, 팔과 다리의 연동을 표현하기 위해 설계 되었다. 환자들이 자유롭게 걷게 하기 위해서(자신이 걷는 것처럼 느끼게 하기 위해서), 이 로봇은 사용자의 움직임과 사지를 움직여 주는 부분 사이의 토크에 대한 상호관계를 계산함으로써 다양한 지형 모양의 변화에 맞추어 걸음걸이의 속력을 구현할 수 있다. 게다가 이 연구는 팔을 올려주는 기계 부품의 손잡이에 스위치로 가상환경 속에서 회전까지도 구현할 수 있다.

이 재활 로봇의 실험적인 결과는 장애인이 걸을 때의 상반신과 하반신의 움직임을 통해 평지와 경사 그리고 계단 등에서 상황에 맞추어 걸음걸이 속력을 변화 시킬 수 있다는 것이다. 그리고 사용자는 속도를 변화 시켜가며 가상 세계를 돌아 다닐 수 있고 회전을 가미함으로써 다양한 움직임의 재활 훈련이 가능하다.

Chapter 1

1 Introduction

1.1 Human Gait Characteristics

Gait simply means “a person’s manner of walking”, which is often interchangeable with walking itself. Walking is body’s natural means of moving from one place to another and the most convenient way of travelling in short distance [1]. The functional versatility, allows the lower limbs to accommodate not only level walking, but also uneven terrains such as stairs and slope.

Walking as man’s everyday activity, makes this action is well-known by every normal human being. However, the in-depth explanation of walking itself is nearly unknown except by the persons who have related work in gait analysis. Therefore, this chapter will review the fundamental explanation of human gait characteristics which will be used throughout this thesis.

Walking uses a repetitious sequence of limb motion to move the body forward while simultaneously maintaining stance stability [1]. When body center of mass moves forward, causing the body to fall forward, and then, by placing a foot forward in time, the actual fall is prevented [2]. This happens periodically, one foot to another, and

between the interchange, where both feet are in contact with the ground, body weight transfer occurs.

A review of some common terms is necessary in order to understand the human gait characteristics.

- Gait or Stride cycle: It is based on the actions of one limb. The duration of a stride is the interval between two sequential initial floor contacts by the same limb. A stride consists of two steps, commonly measured from the time of heel contact of one foot until the next heel contact of the same foot [1]. Figure 1-1 shows how step and stride differs.

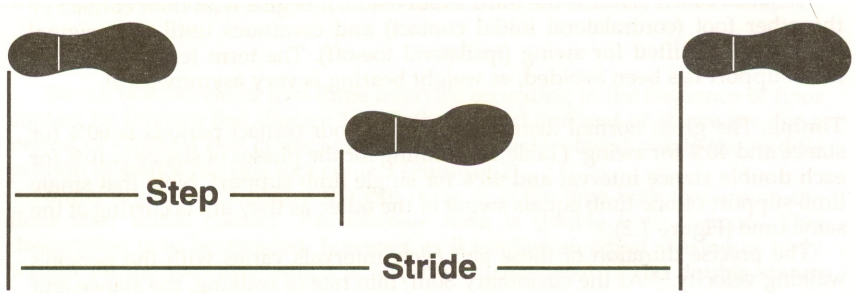

Figure 1-1 Step and stride in a gait cycle [1]

- Phases of Gait: Pattern of motion related to a different functional demand in a gait cycle. Basically, a stride cycle is divided into two periods, stance and swing. Stance is the period when the foot is in contact with the ground and swing is the time when the foot is in the air. When both feet are on the ground is called double stance, which occurs during the interchange between the swing and stance period. The gait cycle can be further divided into three tasks; weight acceptance, single limb support and limb

advancement. These tasks then can be divided into eight phases of the gait cycle, where each phase corresponds to the functionality to accomplish the required task [1]. Figure 1-2 explains the divisions of the gait cycle and Figure 1-3 shows the phases of the gait cycle.

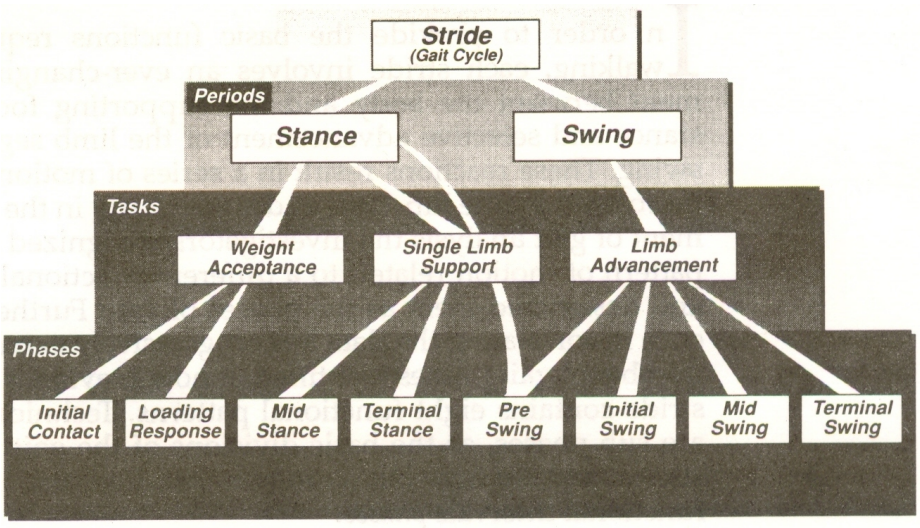

Figure 1-2 Divisions of the gait cycle [1]

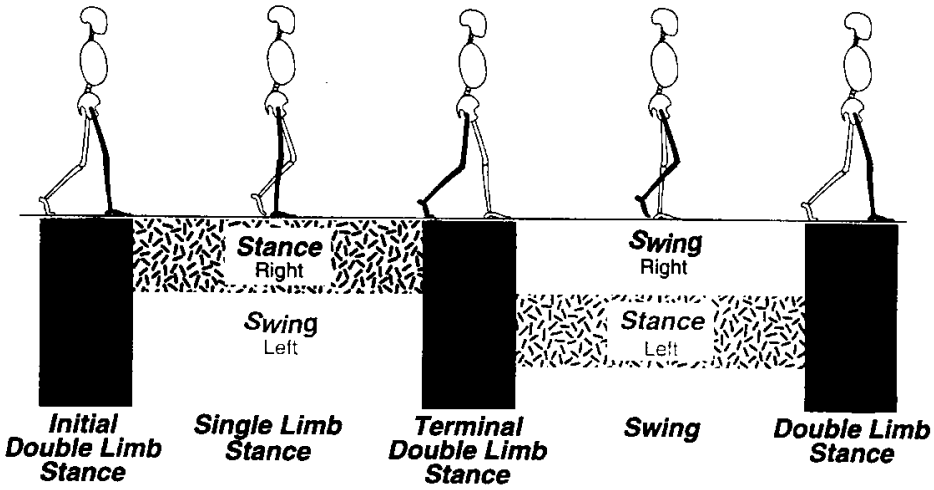

Figure 1-3 Human walking phases in single gait cycle [1]

- Timing/Cycle Time: In a gait cycle, the gross normal distribution of the stance to the swing period is 60 percent to 40 percent. Where in the stance period, the double stance period takes 10 percent between the interchange of swing to stance period and vice versa, see Table 1-1 [1].

Table 1-1

Floor Contact Periods [1]		
Stance		60%
Initial Double Stance	10%	
Single Limb Support	40%	
Terminal Double Stance	10%	
Swing		40%

1.2 Gait Disorders due to Stroke

The list of gait disorders are too long to be discussed here and can be read elsewhere [3]. However, gait disorder due to stroke has been explored numerously using gait rehabilitation robot and will be the main focus of this research.

A stroke happens when sudden focal (sometimes global) neurologic deficit secondary to occlusion or rupture of blood vessels supplying the brain occurs more than 24 hours (if it less it is called transient ischemic attack (TIA)) [3]. It can be classified into two major categories: ischemic and hemorrhagic.

Ischemic stroke occurs when blood supply to part of the brain is decreased, leading to dysfunction of the brain tissue in that area. This type, which occurs in approximately in 85% of strokes can be subdivided into 3 groups: thrombotic, embolic and lacunar. The causes of each group respectively are due to occlusion of major vessels, cardiac source and small lesions. Hemorrhagic stroke occurs when blood spills on some part of the brain due to ruptured aneurysm, bleeding disorders, anticoagulants and other causes. It is divided into 2 groups: intracerebral which is caused by hypertension and subarachnoid which is caused by ruptured aneurysms and vascular malformations [3].

The characteristics of normal gait and gait following stroke will be obviously different. Several characteristics of hemiparetic gait

following stroke reported are reduced walking speed and longer stance phases, but greater on the unaffected side, foot drop, hip hiking, hip circumduction and asymmetric walking [4], [5].

1.3 Neural Recovery Mechanisms

Several theories based on experiments and facts regarding the mechanisms in neural recovery have been established [6]. However, restitution (true recovery), brain plasticity and behavioral compensation are the mechanisms which are mostly discussed and will be explicated here.

From the meaning, restitution or true recovery is when the affected neuron caused by the lesion (depend on its severity) returns to its original functions or to the pre-lesion state. Brain plasticity is the functional reorganization of the CNS (Central Nervous System) of the unaffected neuron [7]. The brain plasticity occurs by the process called synaptic routing and other two similar mechanisms, first is the process of unmasking of existing but functionally inactive path-ways, and second is the use of alternative functional pathways that involve the normal system of cerebral circuit redundancy [6]. Behavioral compensatory is emersion of new movement strategies as a result of correcting the post-lesion movement in order to accomplish a specific task [6]. One example of behavioral compensation is when a right-hemiparetic subject was asked to reach an object located in front of him by his right arm, a rotation by the trunk would give

another degree of freedom and help accomplishing the specific task [8]. These neuronal recovery mechanisms are believed to be important aspects on deciding of how should the gait rehabilitation training is realized. Therefore, a brief explanation regarding this issue is necessary and will be discussed on the following paragraph.

The degree of lesioning caused by the brain damage can be classified into mild, moderate and severe lesion. In mild lesion, rehabilitation is not necessary, because of the spontaneous neuron recovery. In moderate lesion, restitution or true recovery of the neuron may be possible given appropriate type, timing and frequency of inputs [9]. However, for the severe lesion, only brain plasticity and behavioral compensation are possible. Figure 1-4 is showing the degrees of lesioning caused by brain damage.

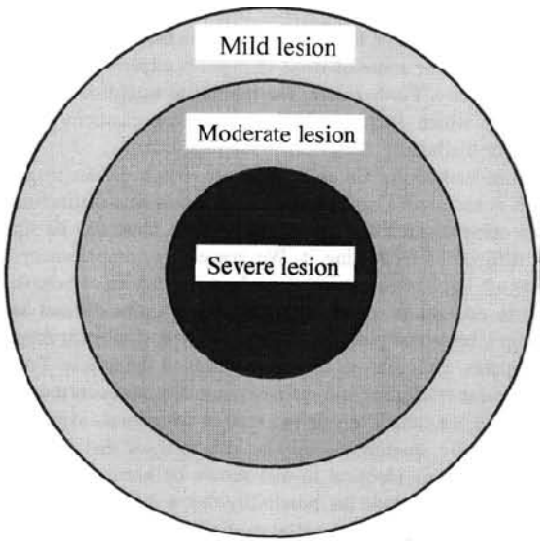

Figure 1-4 Classification of different degrees of lesioning caused by brain damage [9]

Based on the already mentioned recovery mechanisms, we can determine the type of exercise that we want to approach with. In conclusion, the training exercise can be divided into two categories: guided and restrained training. One brief example can be seen from the case study of right-hemiparetic subjects [8]. Training by supporting the trunk rotation could be one of the solutions in giving the patient "ability" to accomplish the desired task. This is called the behavioral compensation mechanism. However, by constraining the motion of the trunk and by only allowing the movement of the arm will be the basis of true recovery or brain plasticity mechanism. In gait rehabilitation training, repetitive motion of the lower limbs is one of the ways to induce the brain plasticity. True recovery mechanism could be realized by restraining in some portion of the gait cycle which is particularly affected, for example the step-height during swing phase. By allowing the foot to gain normal height during training while allowing the unaffected foot to walk normally will effect only on the neurons pertaining the specific functions. In behavioral compensation, gait training by the support of the unaffected foot is necessary to attain more stable walking or by moving the upper portion of the body to change the center of the mass position. This type of exercise usually can be seen in manual training using walker or parallel bar.

1.4 Manual Rehabilitation

The main motivation of gait training is to help a patient recovering from injury, illness or disease, to attain a natural human gait for normal life and to assist the patient in compensating for deficits that cannot be treated medically.

Manual treadmill training, with the body weight partially reduced using a body weight support system, has had significant success in helping chronic non-ambulatory hemiparetic patients improve their gait ability [10], [11]. The major limitation of a manual therapy treadmill as a daily routine is the required involvement of two or three therapists in assisting the gait of severely affected subjects by setting the paretic limb and controlling trunk movements [12]. Figure 1-5 shows the manual treadmill training. At least one physical therapist is needed for each leg with an addition of a therapist holding the body of the patient to keep the center of the body in the middle of the treadmill.

Figure 1-5 Manual treadmill training with body weight support system. The picture on the right is from http://www.drmc.org/images/rehab3.jpg

1.5 Gait Rehabilitation with Robotics Devices

Several groups have developed gait rehabilitation robots to overcome these drawbacks. These robots are able to help the therapists by assuming the task of ensuring repetitive motion while simultaneously helping the patient attain a more precise natural gait.

Figure 1-6 Lokomat (Left), AutoAmbulator (Middle),
POGO & PAM (Right)

There are two major approaches to gait rehabilitation in which the body weight is reduced: treadmill training and training with a programmable end-effector. In treadmill training, the patient walks on a treadmill while wearing the robotic device. This robot helps the patient generate the appropriate walking gait trajectory. This technique is used by the Driven Gait Orthosis (DGO) group [13]. Another training technique is used by the Mechanized Gait Trainer (MGT) group [14] (Figure 1-7). In this technique, the foot is permanently attached to an end-effector that generates a human-like walking pattern. In this training technique, the body weight is also partially reduced. These groups have extended their research based on their previous successes. The Lokomat (Figure 1-6) [15], from the DGO group, is able to adapt the gait trajectory in real-time. The adaptation scheme is based on the interaction between the human leg

and the orthosis. The MGT group has developed the HapticWalker (Figure 1-7) [16], a programmable foot device that is capable of simulating level walking, stairs and stumbling.

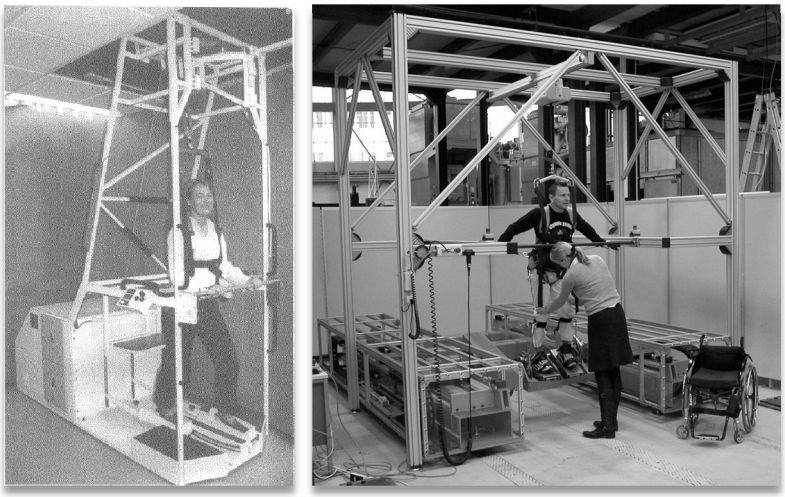

Figure 1-7 Gait Trainer (Left) and HapticWalker (Right)

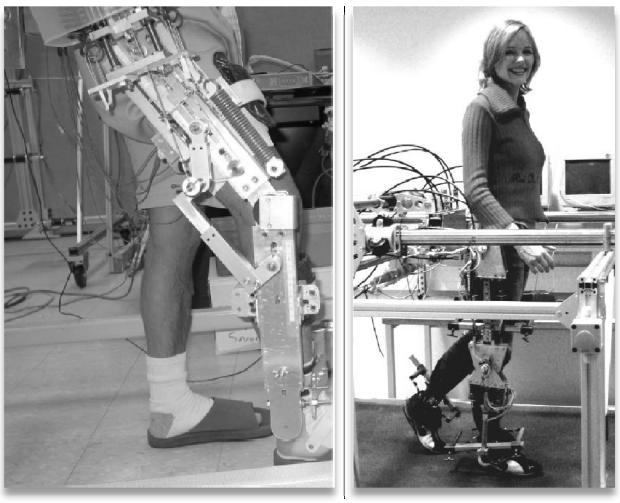

Figure 1-8 Gravity-Balancing Orthosis (Left) and Lopes (Right)

Several robotics devices are now commercially available. These include the AutoAmbulator (Figure 1-6) (HealthSouth Cooperation) and LokoHelp [17] that are sufficiently compact to allow gait training at home. Another robotics orthosis, Lopes [18] (Figure 1-8), based on treadmill training has also been developed. Unlike Lokomat, this orthosis allows the sideways and forward/backward motion of the pelvis. A pneumatically controlled gait orthosis (POGO) and pelvic assist manipulator (PAM) (Figure 1-6) [19], have also been reported. Automatic treadmill speed adaptation [20] has been developed where the adaptation is based on interaction forces applied by the user at the trunk connection. An orthosis (Gravity-Balancing-Orthosis) [21] that is able to reduce the gravity effect to assist hemiparetic patients has also been developed (Figure 1-8). Successful gait rehabilitation system with a locomotion interface has also been reported [22] for

walking training on virtual terrains. This system with two footpads could generate pre-recorded motion sequence to move the user's feet. In the latest development of these robotics devices, however, there has been no report of a device that is able to simulate uneven terrains with ability to update the walking trajectory.

1.6 Virtual Reality in Gait Rehabilitation

The combination of virtual reality (VR) and rehabilitation has given several advantages. One important advantage is that VR can be used to simulate a variety of circumstances that are similar to the real environment, including slope, stairs and obstacles. Another advantage is that the virtual environment (VE) will motivate the patient to train and not feel confined in the physical environment as in traditional gait training, which is usually tiring and tedious. Therefore, if a gait rehabilitation robot can generate various terrain types to realize real walking environments and allow walking navigation in VEs through real walking, the rehabilitation performances will be enhanced. Successful implementation of rehabilitation with VR has been reported for stroke patients [23], in gait rehabilitation [24], [25], [26] and recently Lokomat with healthy subjects [27]. To the best of our knowledge, however, no one has ever implemented walking navigation according to user's intention in VE for gait rehabilitation, an aspect that requires a walking user to execute a walking velocity change and a turn. Even though in

locomotion interface applications, several devices [25], [28], [29], [30] have been suggested for straight walking and turning capability for realistic planar walking navigation, these machines will make the mechanical system complex and not easy to guarantee the safety of patients for gait rehabilitation. Thus, it is necessary to allow a patient to navigate on various terrain types through real walking and to generate a turning command without real turning motion through complex mechanical systems.

1.7 Research Outline

From the literature studies of the existing rehabilitation robots and in the advances of rehabilitative strategies, problems and goals of this research can be explicated as follows:

a. Problem definition

1. Currently, the exoskeleton based type training, Lokomat, has enabled the patient to walk according to his intentions not only to follow the robot movement. However there has been no report for the end-effector based type training that enables the patient to influence to robot's motion according to the patient's intention.
2. To the best of our knowledge, there has been no report in rehabilitation training incorporating interactive virtual reality navigation, which enables the patient to do turning motion in virtual environment using an input device.

3. Our hypothesis is that, by providing the patient the real feeling of walking, while also synchronizing to virtual reality where the patient can navigate inside the VE, might give higher benefit to the outcome of gait rehabilitation training.

b. Research goals

1. To realize a programmable footplate-type gait rehabilitation robot that allows walking velocity update through human robot interactions.
2. To develop a virtual environment where the user can interactively navigate inside the VE through an input device.
3. To combine an immersive effect of virtual reality with real walking (level walking, stairs and slope) which are generated by the foot device, while also allowing walking velocity update inside the virtual reality.

1.8 Thesis Outline

This thesis describes the design, control and VR navigation of a novel 6-DOF gait rehabilitation robot that allows walking velocity update on various terrain types and navigation inside a VE through upper- and lower-limb connections. We introduce a basic concept of upper- and lower-limb connections in Chapter 2. In Chapter 3, we describe the development of the suggested gait rehabilitation robot that allows upper- and lower-limb connections on various terrain

types. In Chapter 4, we provide the walking interaction control scheme with a synchronized walking pattern and a walking velocity update algorithm. In Chapter 5 we describe the navigation algorithms. We provide our experimental results in Chapter 6. In Chapter 7, we present our conclusions and a discussion of future work.

Chapter 2

2 Gait Rehabilitation with Upper- and Lower-Limb Connections

2.1 Neuronal Connections of Human's Upper- and Lower-Limb

Current gait rehabilitation robots only enable lower limb motion without considering the coordination of leg and arm movement. As a matter of fact, muscle activity controls the magnitude and timing of arm swing during human locomotion [31]. The arm to leg cycle frequency during walking has already been found to be one to one ratio [32]. Humans recruit upper limb muscles to swing their arms at a much faster rate than the arms' natural frequency during running, and become slower during slow walking. As humans change walking speed, their nervous systems adapt muscle activation patterns to modify arm swing for the appropriate frequency [33]. Furthermore, it has been known that the arm swing during human locomotion also helps stabilize rotational body motion [34].

Although a complete explanation of the neuronal connection between the upper and lower limbs has not yet been developed, several research studies have shown that there exists a neuronal coupling between arms and legs during locomotion. A gating function of neuronal pathways between upper and lower limbs was proposed

by Dietz et. al. based on treadmill experiments and evaluation of the effect of small leg displacements on leg and arm muscle electromyography activity in walking humans [35]. More recently, studies on neurogically intact subjects have demonstrated an increase in lower-limb muscle activation that is proportional to upper-limb muscle use during seated recumbent stepping [33], [36], [37]. Figure 2-1 shows an overview of neuronal connection of human arms and legs related to robot- upper and lower-limb interaction.

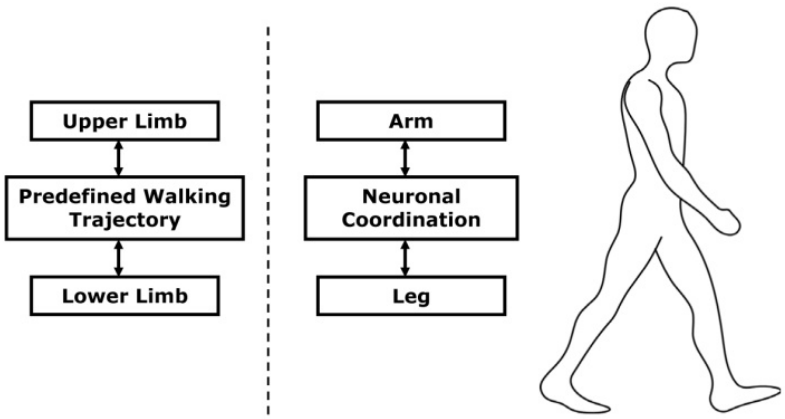

Figure 2-1 Neuronal connections of humans' arm and leg related to the robot's lower and upper limbs interaction

2.2 Facilitating Arm Swing in Locomotor Training

For implementation of various rehabilitation modes [38], it is desirable that a patient walks at will, and not just by following the movement of a robot. In the programmable foot plate training method,

even though various terrain trajectories can be generated, the large inertia of the robotic manipulators makes interactive control between the human foot and robot difficult to implement [39], due to inability to provide low impedance with position-based control. However, in our robot, the walking update can be implemented based on the interaction of the human upper limbs and the robot arms which can allow walking velocity change regardless of robot manipulator's size and difficulty to implement interaction control between human foot and manipulator. Moreover, a recent research has also reported that facilitating arm swing could be beneficial in locomotor training [40]; thus providing arm swing will give better results in the gait training.

Chapter 3

3 Gait Rehabilitation Robot with Upper- and Lower-Limb Connections

In this thesis, we suggest a novel 6-DOF gait rehabilitation robot to allow upper- and lower-limb connections and to allow walking training on various terrain types. The main design objective is to develop the dexterous, compact, and inexpensive rehabilitation robot for the purpose of telerehabilitation [41]. Our robot system consists of three parts: the lower limb composed of a sliding device and programmable foot device, the upper limb and the body support system. Each part is explained in following subsections. Also, the control strategies of each actuator to track the designed trajectories and to ensure the stability and the safety of the system will be described. Finally, the control hardware and software for the developed robot will be explained. Figure 3-1 shows a three dimensional (3D) model of the proposed gait rehabilitation robot. The coordinate system used in this design: x+ axis points to the front side, y+ axis points from the ground to upside, while z+ axis points to the right side of the device.

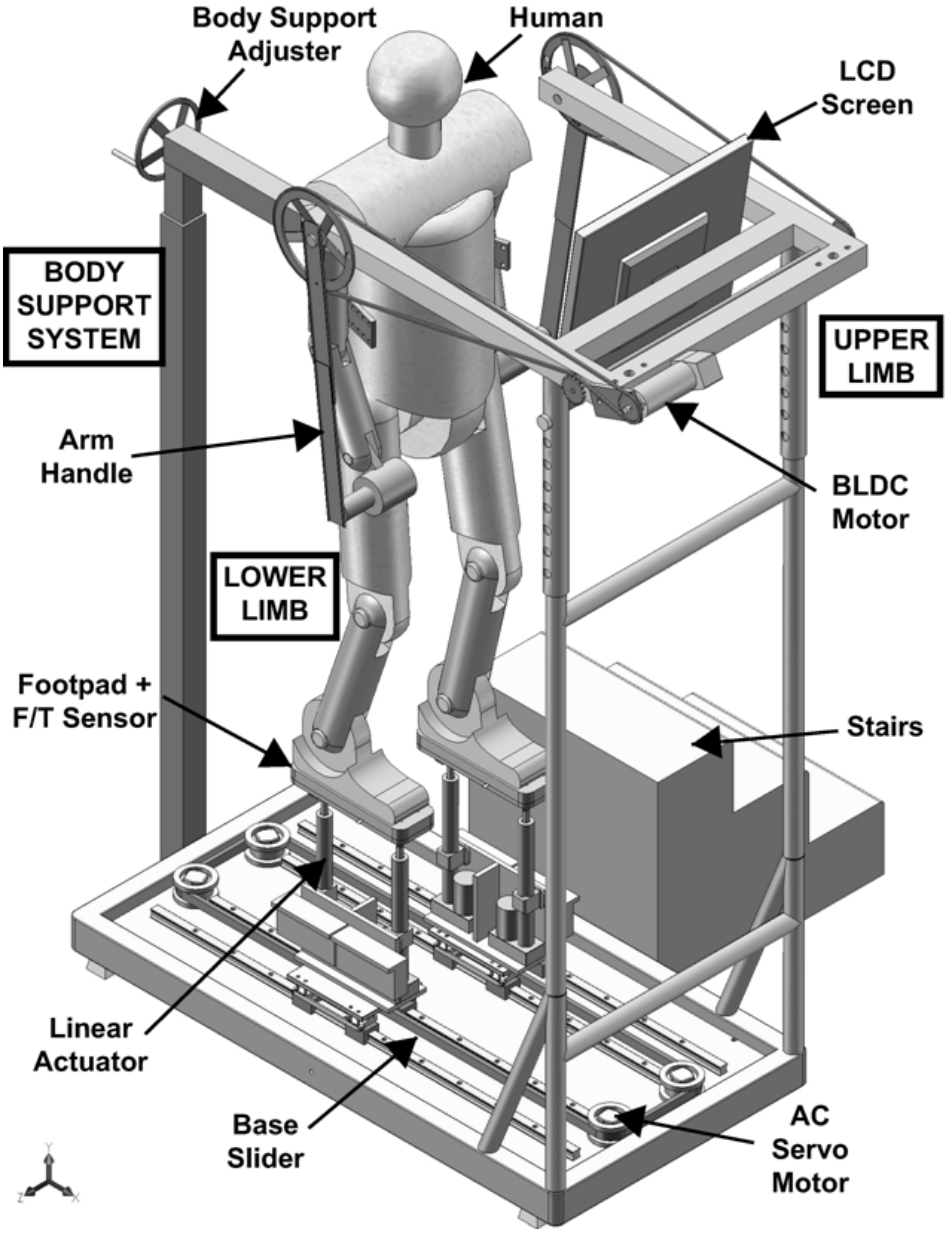

Figure 3-1 Overview of the gait rehabilitation robot

3.1 Mechanical Design

3.1.1 Footpad Mechanism

The design of our rehabilitation robot enables us to simulate different terrain types, such as walking on level ground, stairs and slope. The robot is designed so that it is able to carry the entire human weight during locomotion. The mechanism of the foot end-effector uses a parallel mechanism that offers greater stiffness than a serial mechanism.

Two linear actuators (P1 and P2) are arranged in parallel and connected together by a footplate with revolute joints as shown in Figure 3-2. An additional prismatic joint P3 is located between R1 and R2 joints. This mechanism is a new type of five-bar mechanism with two prismatic actuators which are fixed to the ground. Thus, these two actuators can generate spatial motions of toe and heel parallel to y-axis. Figure 3-2 shows the 3D model and schematic diagram of the footpad.

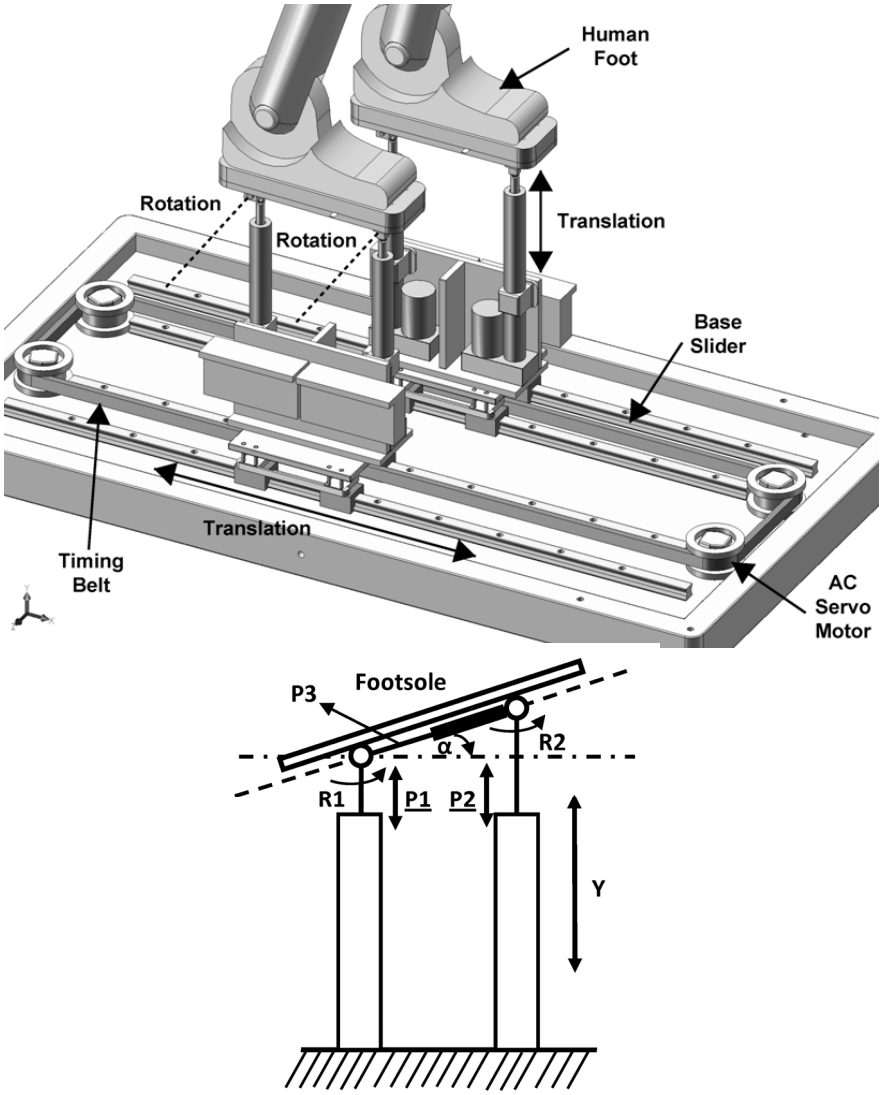

Figure 3-2 3D model of 3-DOF foot platform (top) and schematic diagram (bottom)

3.1.2 Slider Mechanism

A 1-DOF slider mechanism is used for the x-axis motion. The slider is connected to a timing belt driven by an AC servo to ensure the feet move in opposite directions at the same velocity. The symmetric walking on programmable platform devices can reduce the excessive movements of the center body of a user [42]. Treadmills may not adequately cancel the stance foot velocity during walking on a treadmill because the treadmill can generate only a constant velocity for the stance foot during the gait cycle, even though the swing foot velocity is not constant during the swing phase. Thus, the symmetric walking concept for programmable foot platforms will allow more stable walking in the suggested slider device. For symmetric walking, only one motor at the base slider is required as shown in Figure 3-3, reducing the complexity of requiring two motors used to generate right and left foot motions. Thus, the full end effector for each foot will have 3-DOF motion in the sagittal plane.

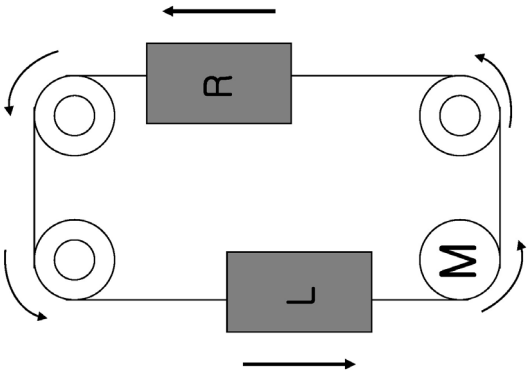

Figure 3-3 Base slider mechanisms

3.1.3 Upper Limb

Humans swing their arms when they walk or run to maintain stability. Several researchers have described arm swing in the sagittal plane using a pendulum model [43], [44]. Although the arm swing itself is not exactly passive phenomenon [33], the motion of the shoulder can be simplified as a single-link pendular motion. In this robot, the two arm links are located parallel to the human shoulders on the axis of the shoulder joints, and these are connected through a chain-and-sprocket mechanism These two links are connected to a shaft so that they move opposite each other to simplify the mechanism and ensure synchronization of the upper- and lower-limb for symmetric motions.

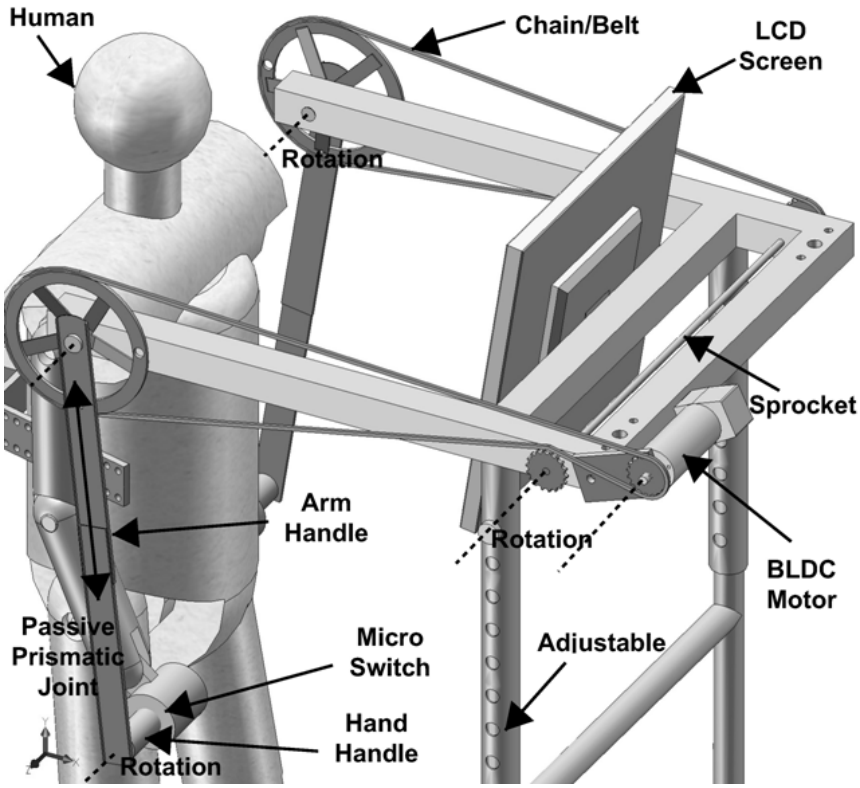

Figure 3-4 3D model of the upper limb

There is a handle located at the end of each arm link for the patient to hold and follow the movement of the robot arm. The position of the upper-limb portion can be adjusted according to the patient's height to provide a comfortable position during training. The robot arm handle has a prismatic joint to accommodate arm movement when walking, to interact smoothly with the human elbow joint. Limit switches on both handles are installed as input devices for VR navigation. Figure 3-4 shows a 3D model of the upper limb part.

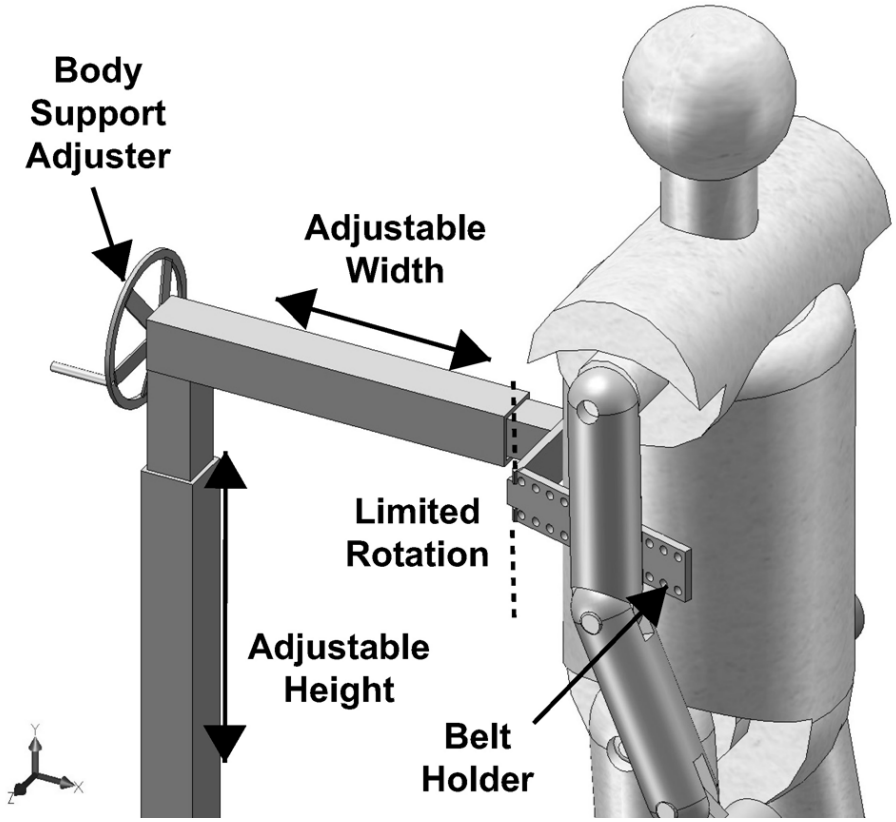

Figure 3-5 3D model of the body support system

3.1.4 Body Support System

A simple support system was designed to hold the body of the patient. The support system can be adjusted according to the patient's height, waist size, and step length. A safety belt is fastened on the patient's waist and connected to a belt holder that has limited degrees of freedom. With this scheme, the body is not fully fixed, but

given some freedom for sideways motion. This mechanism prevents the body from falling forward or backward, and keeps the middle of the body centered since the slider motion is symmetric. In the future, a body weight support system will be provided to accommodate a patient who cannot stand alone. Figure 3-5 shows a 3D model of the body support system. Finally, the mechanical specifications of the developed gait rehabilitation robot are listed on Table 3-1.

Table 3-1

Mechanical Specifications

Attribute	Specification
Length	1.35 m
Width	0.68 m
Height	2.2 m
Maximum Step Height	0.18 m
Maximum Step Length	0.8 m
Arm Swing	45 deg (max. length 0.7 m)
Maximum Walking Velocity	0.3 m/s
Max Payload	75 kg

3.2 Safety Systems and Electronics Requirements

3.2.1 Matlab Simulation

Before the experiment took place, a kinematics simulation using Matlab, Simulink, Simmechanics and VRML Toolbox had been done [45]. The simulation's purpose was as preliminary test and to give a brief idea of how the trajectory synchronization and control algorithm should be implemented. Thus, the safety of the device can be considered before the manufacturing of the robot. Figure 3-6 shows the snapshot of the VRML view of the simulation.

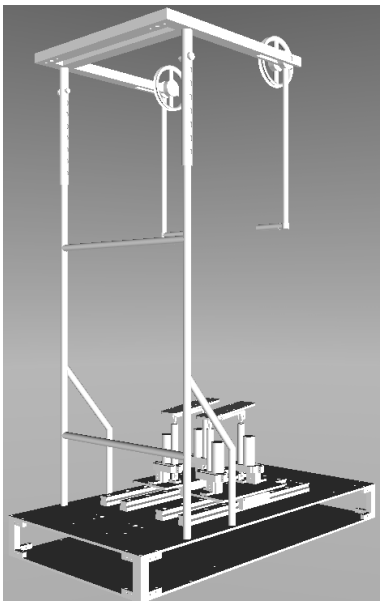

Figure 3-6 A snapshot of VRML view of Matlab simulation [45]

3.2.2 Robot Safety

Figure 3-7 is showing the safety switches of the robot located at the end of the right side of the base slider. Total 4 switches, 2 switches functioning as limit switch connected to the controller input for direction signal, and 2 other switches functioning as safety switch which are hard-wired to the disable input of inverter of the AC servo motor. These disable switches if activated, will disable the actuators and send a disable signal to the controller. For additional safety, the encoders of the AC servo motor and the BLDC motor are limited to a certain value, so that if the encoder value is beyond that limit, a disable signal will be generated and halt the system immediately.

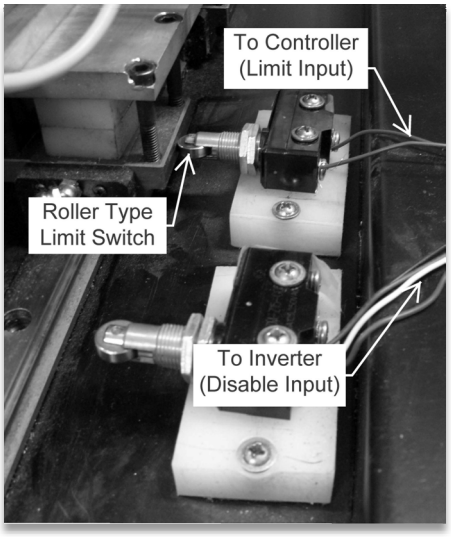

Figure 3-7 Safety Roller Switches

3.2.2 Electronics Specifications

Since the robot must be able to carry the patient weight, a linear actuator with potentiometer feedback and maximum load-carrying capacity of 75 kg, is selected. The linear actuator is actuated with a high speed stepper motor and can reach a maximum speed of 0.18 m/s. A 0.7 kW AC servo motor with encoder feedback is utilized for the slider device. For the upper limb, a Maxon 250 watt brushless DC motor with gear reduction (maximum torque: 25 Nm) and built-in encoder is installed in the middle of the upper limb part.

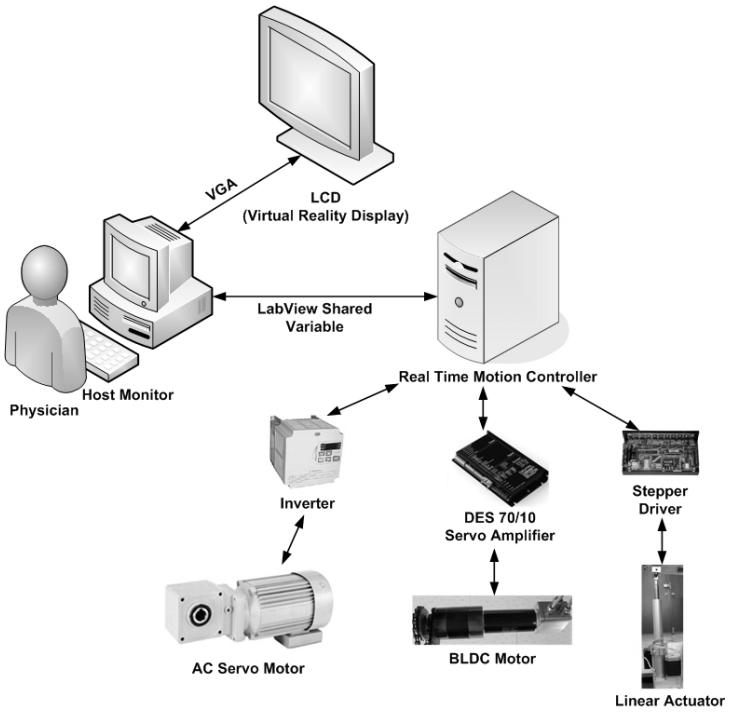

Figure 3-8 Overview of the control systems

We use an eight-axis motion controller from National Instruments, programmed in LabView Real-Time (LV-RT), for hardware and software real-time control. There are two computers in the system. The first one is a monitoring computer on which the therapist can change the training parameters and monitor the training conditions, and the second one is for the embedded program running on LV-RT operating system. Figure 3-8 shows the overview of the control systems.

Table 3-2

Electronics Requirements and Specifications

Electronics	Qty	Specifications
AC Servo Motor	1	0.75 kW, 1740 rpm
Linear Actuators	4	16 in/sec
BLDC Motor	1	250 W, 8380 rpm
Inverter	1	1 HP, 0.75 kW
Stepper driver	4	7080, Applied Motion
BLDC Motor Driver	1	Maxon DES 70/10
Encoder	1	2500 qc
Motion Controller	1	NI -PXI 7358
DAQ Card	1	NI-PXI 6259

3.3 Actuator Control

Since disturbance forces due to the body weight are changing during human locomotion and also some parameters of the robot dynamics such as friction and damping are uncertain, the sliding mode control [46] is chosen as the robust controller of the sliding device and the upper limb device. The linear actuators for the footpad device are controlled through pulse step control using trajectory generator functions provided by the motion controller. These three actuators are independently controlled and tuned manually to achieve the minimum error for the predefined trajectories.

For BLDC motor control of the upper-limb device in torque mode, the proportional integral sliding mode control (PISMC) sliding surface [46] is defined as:

$$s = K_p\tilde{\theta} + K_i\int_0^t \tilde{\theta}\, dt + \dot{\tilde{\theta}} \tag{3.1}$$

where,

$$\tilde{\theta} = \theta_m - \theta_d \tag{3.2}$$

$\tilde{\theta}$ is the tracking error, θ_m is the actual position, and θ_d is the desired position, K_p , K_i and φ_u are the control parameters. The final controller is derived as:

$$I = I_{eq} + I_{switching} \tag{3.3}$$

where,

$$I_{switching} = -n\ sat(\frac{s}{\varphi_u}) \tag{3.4}$$

and I is the current control input to the servo amplifier, n is the control parameter, I_{eq} is the control law to maintain $\dot{s} = 0$, and $I_{switching}$ is the high frequency control laws to force the output towards the sliding surface, and φ_u are the chosen small constants value (boundary layer) to reduce the chattering effect.

For the AC servo motor of the sliding device, utilizing frequency control of the inverter, the SMC sliding surface [47] is defined as:

$$s = (\frac{d}{dt} + \lambda)^{r-1} \tag{3.5}$$

where,

$$\tilde{\theta} = \theta_m - \theta_d \tag{3.6}$$

$\tilde{\theta}$ is the tracking error, θ_m is the actual position, and θ_d is the desired position. While the final controller is:

$$V = V_{eq} + V_{switching} \tag{3.7}$$

where,

$$V_{switching} = -K\ sat(\frac{s}{\varphi_l}) \quad (3.8)$$

and V is the control input voltage to the inverter, r is the order of the AC servo motor dynamics, K, λ and φ_l are the control parameters. V_{eq} is the control law to maintain $\dot{s} = 0$ and $V_{switching}$ is the high frequency control law, and φ_l is the boundary layer. Thorough derivation and proof of stability of the controllers are described in Appendix A.

3.4 Real-Time Program Architecture

We utilize LabVIEW real-time v8.5 on a dual core CPU to control the robot. The program is mainly divided into three loops with different rate due to the different inherent response of each actuator. The 1st and 2nd loops are time critical and assigned to individual CPUs (0 and 1), while the 3rd loop is less time critical and being managed by the LabVIEW Real-Time operating system. The maximum rate of the actuator control that can be achieved is 111 Hz and considered to be enough for the purpose of position control. For the objective of data collection, data is sent autonomously through real-time shared variable to the host computer. In the host computer, the data received is then displayed to the LCD screen for monitoring by the therapist and can be saved to a text file. Thus, the real-time OS will strictly function as controller only. Besides doing data collection, the host computer will also function as virtual reality controller.

The 1st loop with 125 Hz loop rate, is handling the real-time communication between real-time OS and host, encoder limits and roller switches for safety, micro switches signal for navigation and robot-user interaction torque calculation. The 2nd loop contains the sliding mode control of the AC servo motor and BLDC motor. The rate of this loop is 111 Hz. The 3rd loop is handling the control of the 4 linear actuators and has the lowest rate 40 Hz. The program GUI and flowchart are shown in Appendix B.

Chapter 4

4 Walking Interaction Control for Upper- and Lower-Limb Connections

This section describes the walking pattern that synchronizes the motion of the upper and lower limbs and generates walking trajectories on level ground, stairs, and slopes It is not easy in programmable footpad devices to allow velocity updates from a patient through impedance control [15] as Lokomat does because a robotic manipulator must have a high inertia and the backlash of reduction gears to carry the full human weight. A manipulator with high inertia and backlash is usually not reversible and has difficulty achieving low impedance [39]. Since humans swing their arms during normal walking, adding an upper-limb device for natural swinging allows natural interaction between the robot and human arms during walking. Since the upper and lower limbs move at the same period [32], the lower-limb walking velocity will be updated naturally. The method is fairly simple and is described in this section.

4.1 Walking Pattern Synchronization

Three different trajectories are predefined for the upper limb, x-axis motion, and y-axis motion to imitate normal human walking.

These trajectories are designed with the same period so that each will coincide at the end of the walking step.

The parameters used in achieving the same step period are the step length and the walking velocity. A period of one step is

$$step\_period = \frac{step\_length}{walking\_velocity} \tag{4.1}$$

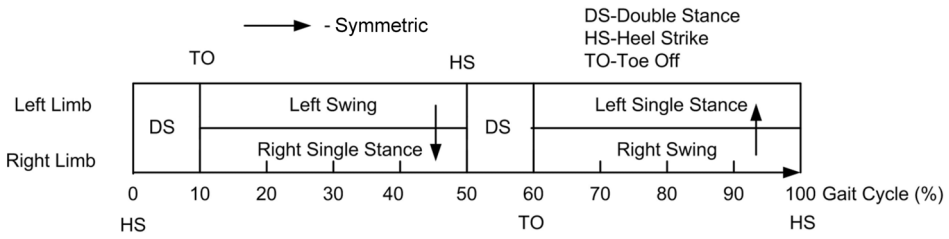

Figure 4-1 Symmetrical walking during one gait cycle

The trajectory was designed using a quintic polynomial [48] to achieve a smooth curve and to prevent shocks in the x-axis direction. In a normal human gait, the proportion of swing to stance phase is 40%-60% of one gait cycle [1]. The initial 10% and final 10% of the stance phase are the double stance. The single stance phase (40%) can be matched to the swing phase of the opposite foot. Thus, if the stance foot for control input is driven by the opposite swing foot as shown in Figure 4-1, symmetric motion between the stance and the swing foot can be maintained since the periods of the swing phase and the single stance phase are the same. The

magnitudes of the swing foot and the stance foot are also the same although they have different directions [42].

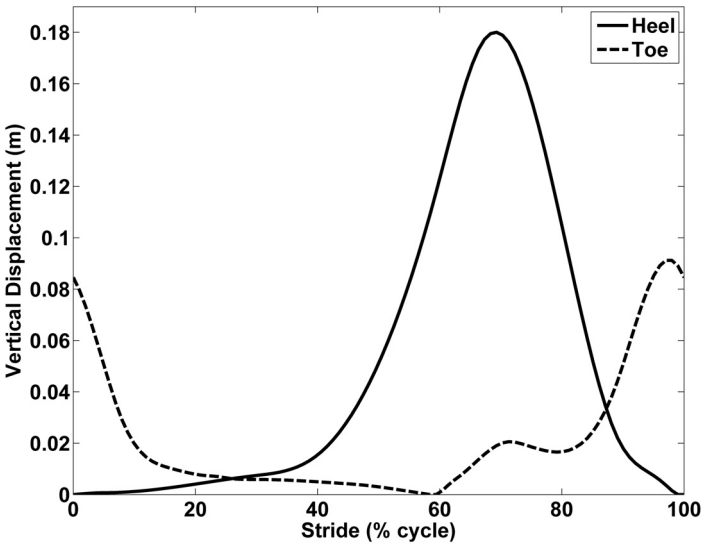

Figure 4-2 Toe and heel trajectory of level walking

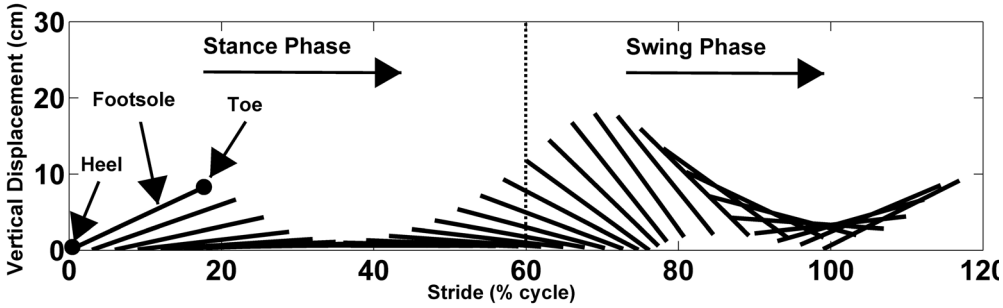

Figure 4-3 Toe and heel positions of one stride during level walking

The y-axis trajectory of level walking consists of toe and heel motions. This trajectory is adapted from one research paper which studied the foot trajectory of human gait [49]. The step period can

be calculated for each different walking velocity. The toe and heel positions can be found as a function of the step period using cubic spline interpolation, as shown in Figure 4-2. Figure 4-3 shows a foot trajectory with toe and heel positions on level walking during one gait cycle.

The upper-limb motion is based on a simple pendulum model. This is a sinusoidal trajectory that is a function of arm frequency and maximum amplitude. The maximum amplitude is the maximum human arm swing angle, and the arm frequency is reciprocal of twice the period of one step:

$$arm\_freq = \frac{1}{2 * step\_period} \tag{4.2}$$

Hence, the angle for each arm swing can be calculated by:

$$\theta(t) = \max\ \_amplitude * \sin(\omega * t) \tag{4.3}$$

where,

$$\omega = 2 * \pi * arm\_freq \tag{4.4}$$

Using trajectory analysis, the motions of the upper and lower limbs are synchronized in the same period to maintain the normal human walking pattern, since the humans arm and legs are also moving together at the same frequency [32]. Figure 4-4 depicts the algorithm overview of trajectory generation.

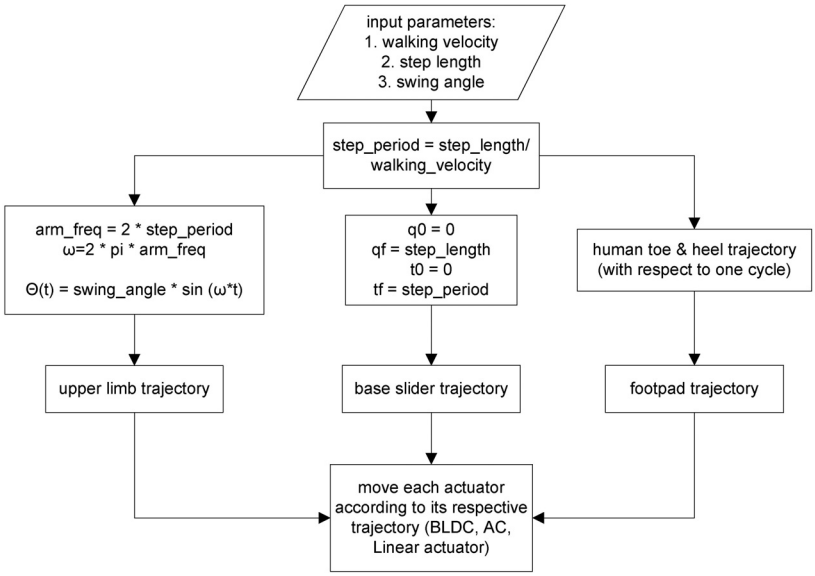

Figure 4-4 The complete diagram of the trajectory design

4.2 Stairs and Slope Trajectory Generation

A locomotion interface based on parallel manipulators is able to generate stair and slope motions [28]. However, since the foot is not permanently attached to the platform, it does not fully support the foot during swing phase. In our system the stairs and slope trajectories are measured from the captured sequence of motions during stair climbing and slope walking, and can be generated for gait rehabilitation during whole gait cycle. The swing to stance phase ratio is approximately similar to level walking, which is near 40%-60% of one gait cycle. Figure 4-5 shows the walking up stairs

trajectory after interpolation with stair height of 6 cm with respect to toe and heel height versus one gait cycle. Figure 4-6 shows the walking up slope trajectory with the slope angle of 10 degree. Figure 4-7 is showing the foot trajectories with toe and heel position during walking up stairs and slope respectively.

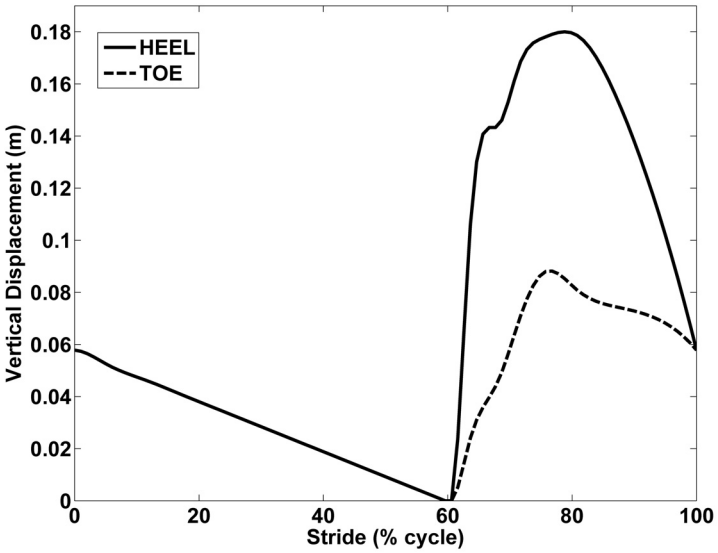

Figure 4-5 Toe and heel trajectory of walking up stairs

Finally, the synchronization scheme of upper and lower limbs during stairs or slope climbing can be similar to level walking since the arm swing and foot step always meet at the same period based on heel and toe positions with respect to one gait cycle.

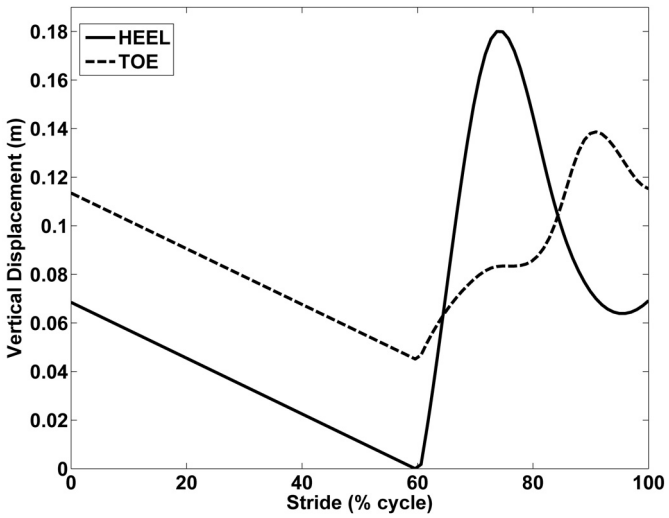

Figure 4-6 Toe and heel trajectory of walking up slope

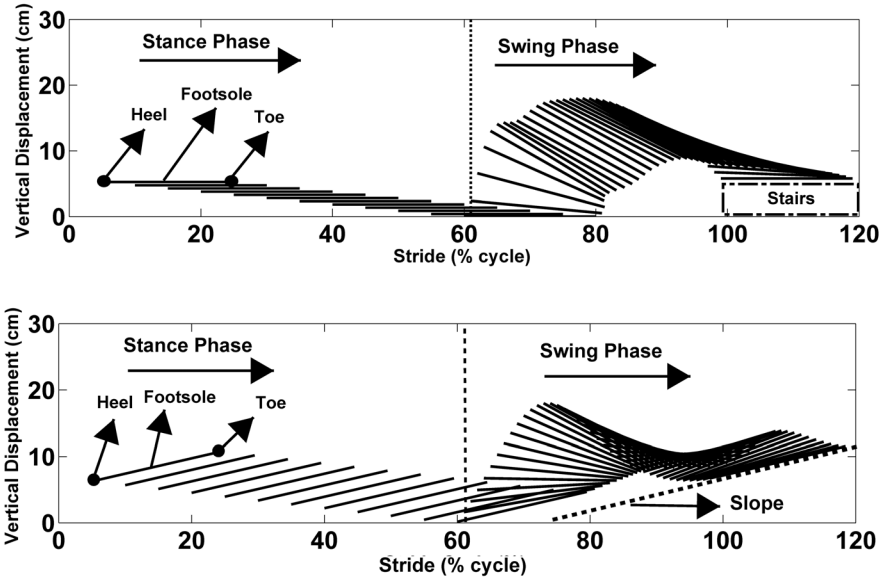

Figure 4-7 Toe and heel positions of one stride during walking up stairs (top) and slope (bottom)

4.3 Estimation of the Interaction Torque

The upper limb is a single pendular motion actuated by a BLDC motor, with a dynamics equation expressed as:

$$J\ddot{\theta}_{act} + B\dot{\theta}_{act} + mgl\sin(\theta_{act}) + T_{d,est} = T_{m,act} \quad (4.5)$$

where,

$$J\ddot{\theta}_{act} + B\dot{\theta}_{act} + mgl\sin(\theta_{act}) = T_{m,est} \quad (4.6)$$

Here, $\ddot{\theta}_{act}$ is the actual acceleration, $\dot{\theta}_{act}$ is the actual velocity, θ_{act} is the actual position angle of arm swing, J is the arm handle inertia, B is the damping coefficient, m is the mass of the link located at the end (arm handle), g is the gravity, l is the arm handle length, $T_{m,act}$ is the actual motor torque, $T_{m,est}$ is the estimated motor torque and $T_{d,est}$ is the estimated disturbance torque which is generated by the human.

By measuring the current directly from the motor, the actual motor torque can be estimated as:

$$T_{m,act} = K_t * I_{act} \quad (4.7)$$

where K_t is the motor constant and I_{act} is the measured current. When the patient is interacting with upper limb device, the estimated $T_{d,est}$ is estimated:

$$T_{d,est} = T_{m,act} - T_{m,est}$$
$$= T_{m,act} - J\ddot{\theta}_{act} - B\dot{\theta}_{act} - mgl\sin(\theta_{act}) \quad (4.8)$$

A threshold value is chosen, since it is not easy to determine the user's intention through small values of $T_{d,est}$. If $T_{m,est}$ is bigger than $T_{m,act}$, the patient tries to move the arm handle faster or with arm swing angle larger and faster than the specified robot's arm angle. Thus, if $T_{d,est}$ is positive, the patient wants to move more slowly; if $T_{d,est}$ is negative, the patient wants to move more quickly.

4.4 The Update of Walking Velocity Algorithm

The walking phases in human locomotion consist of stance, swing and double stance phase. These phases occur in two steps or in one stride. If a walking velocity is changing, there is also a change in frequency between the arms and the legs [43]. Thus, in order to synchronize upper and lower limbs, the control parameter should be the period instead of interaction torque. The period over the threshold value is the desynchronized time between the upper and the lower limbs. The longer the desynchronization happens the bigger the period, and hence it is proportional to a patient's intention when he wants to change the walking velocity. If $T_{d,est}$ is higher than the threshold value, T_{Th}, the period is increased and vice versa. Finally,

the period of the $T_{d,est}$ signal over the threshold will be integrated during one stride. In one stride, this algorithm can be formulated as:

$$N_{T_{d,est}} = \int P_{T_{d,est}>T_{Th}} - \int P_{T_{d,est}<-(T_{Th})} \tag{4.9}$$

$$If\ N_{T_{d,est}} > 0, Vel_{next} = Vel_{cur} + V_{vel}$$
$$Else\ If\ N_{T_{d,est}} < 0, Vel_{next} = Vel_{cur} - V_{vel}$$

where $N_{T_{d,est}}$ is the integrated period over threshold value, Vel_{next} is the walking velocity for the next gait cycle, Vel_{cur} is the current walking velocity, and V_{vel} is the increment/decrement value of the walking velocity. The value of V_{vel} can be defined according to the patient's severity, desire or the training improvement. Thus, in every update of walking velocity, V_{vel} is formulated as:

$$V_{vel} = N_{T_{d,est}} * K_{vel} \tag{4.10}$$

where K_{vel} is a constant to limit the maximum value of V_{vel}.

After each stride, $\int P_{T_{d,est}}$ is reset and the velocity is updated, thus the update of walking velocity takes place once every stride (two steps), not once each step. With this scheme, the patient will maintain the same walking velocity for each stride and the velocity is updated gradually so that the patient will feel stable and comfortable. The update information of the walking velocity will also be transferred into the VE. Since the lower limb trajectories for level walking, stairs

and slopes are based on vertical displacements of heel and toe as a function of walking cycle as shown in Figure 4-2,4-5 and 4-6, the same walking update algorithm are also applicable for walking on stairs and slopes.

Chapter 5

5 Navigation in Virtual Environment (VE)

5.1 Virtual Environment Setup

A simple VE was developed based on the Picture 3D toolkit in LabView. As shown in Figure 5-1, the moon and the building act as the background, and the four boxes are targets.

There are two important aspects of navigation in a VE: the camera position and the target. The camera position is the current user position, while the target indicates the direction in which the user is looking. When walking or turning in the VE, these two information items must be updated according to the position of the foot and the input signal from the switches located at the arm handles of the upper limb device.

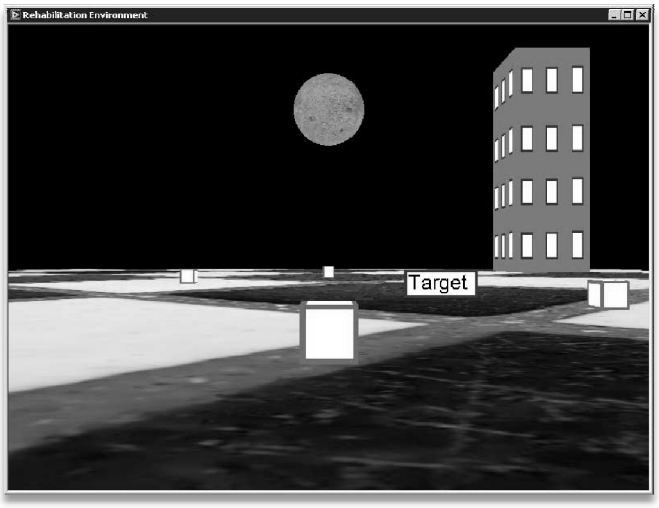

Figure 5-1 The Virtual Environment

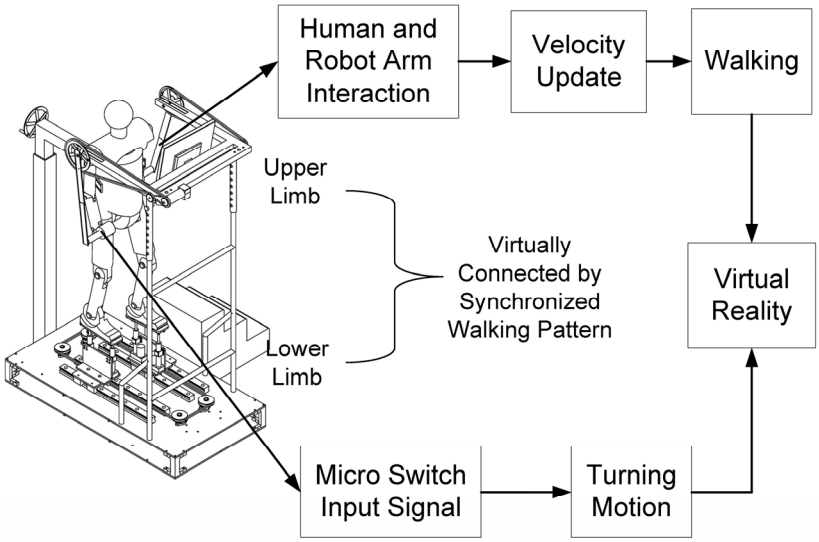

Figure 5-2 Overview of the navigation system with upper- and lower-limb connections

An LCD monitor is mounted on the device to display the VR image. It is relatively inexpensive and there have been no reported occurrences of cybersickness [23]. The LCD monitor is connected to the therapist computer through VGA connector so that both the therapist and the patient can view the VE at the same time. Therefore, the therapist is able to monitor both the training parameters and the perceptual experience of the patient in the VE. The overview of the navigation system with upper- and lower-limb connection is shown in Figure 5-2.

5.2 Straight Walking Algorithm

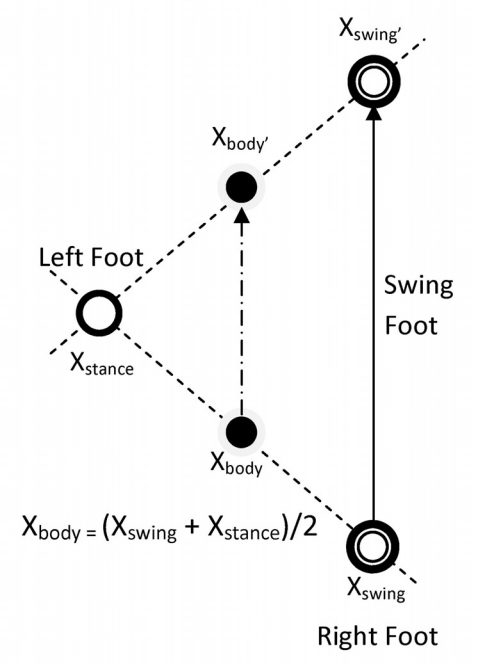

Figure 5-3 Straight walking algorithms

In straight walking, the position of the slider platform is transferred simultaneously from the real-time controller to the host monitor. To synchronize the walking motion with the VE, the foot that is in the stance phase acts as the reference. Figure 5-3 shows the straight walking algorithm in which the left foot acts as reference. The ground position in the VE is updated according to the center position of the body which is located between the two feet. As shown in this figure, the body position moves from X_{body} to X_{body}' as the swing foot will move from the X_{swing} to X_{swing}'. Since the slider motion is symmetric, only one position of the foot (from the encoder) is available at a time. During swing phase of the right foot, the position of the left stance foot can be calculated as:

$$X_{stance,L} = step\_length - X_{swing,R} \tag{5.1}$$

where $X_{stance,L}$ and $X_{swing,R}$ are the x-axis position of the left foot during stance phase and the x-axis position of the right foot during swing phase, respectively. Then, the straight walking algorithm in VE is described as follows:

$$X_{body} = \frac{step\_length - |X_{stance,L} - X_{swing,R}|}{2} * walking\_velocity \tag{5.2}$$

Then in VE:

$$Vel_{X_{cam'}} = Vel_{X_{cam}} + Vel_{X_{body}} \quad (5.3)$$

where X_{cam} is the axis coordinate in the VE. From (5.2) and (5.3), the velocity of X_{body} becomes minimum during double stance phase. If both of the feet are in the middle, the velocity of X_{body} become maximum because of the property of the quintic polynomial trajectory. With this scheme, the motions of the body in the real and VR worlds are synchronized.

5.3 Turning Motion Algorithm

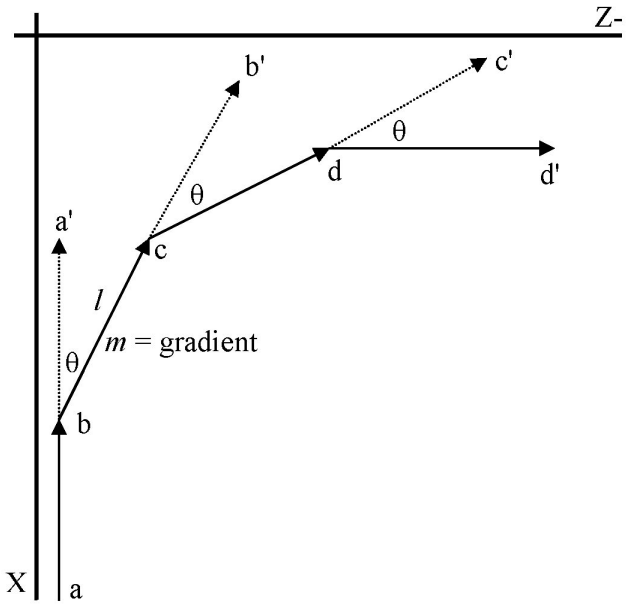

Figure 5-4 Turning motion algorithm

Figure 5-4 shows the turning algorithm scheme with the working VE coordinates in X and Z axes. Initially, the camera position is located at point a, and the target is directed at point a'. Supposed a has coordinates (X_{cam}, Z_{cam}) and a' is has coordinates (X_{target}, Z_{target}), the line l equation is found with the following formula:

$$X = m * Z + p \tag{5.4}$$

where m is its line slope (gradient), and p is the line offset value. The gradient m can be found from:

$$m = \tan\left(\frac{\pi}{2} - \theta\right) \tag{5.5}$$

where θ is a walking direction angle from the switches at the upper limb handle. The switch-on signal at the right handle is proportional to positive angle θ, while switch-on signal at the left handle is proportional to negative angle ($-\theta$). Then, p can be found by substituting X, Z and m in (5.4). At initial time, p is equal to X_{cam} since the angle is zero. When the patient pushes the right switch, the command angle (θ) is increased, and p and m value must be updated. Finally, by applying the straight walking algorithm from equations (5.1)-(5.3), a patient can walk from position b to c, and for this, the value of Z can be calculated from (5.4).

Chapter 6

6 Experimental Results

6.1 Experiment Setup

An experiment has been performed with a healthy subject. The subject weighs 66 Kg and is 170 cm tall. The control parameters chosen for the PISMC of the pendular motion (BLDC motor) are K_p = 15, K_i=0.001, n =0.33, φ_u=1. The control parameters chosen for the SMC of the slider motion (AC Servo Motor) are K=9, λ=15, φ_l=0.05 with the order of system dynamics r=3. At the beginning of the trial, the velocity was set to 0.05 m/s and the subject was asked to change his walking velocity by manipulating the swing motion of the robot arm. The step length defined is 0.4 m, the step height is 0.18 m, the arm swing maximum angle is 15 degree and the threshold value T_{Th} is 1.5 Nm. Figure 6-1 shows the experimental setup.

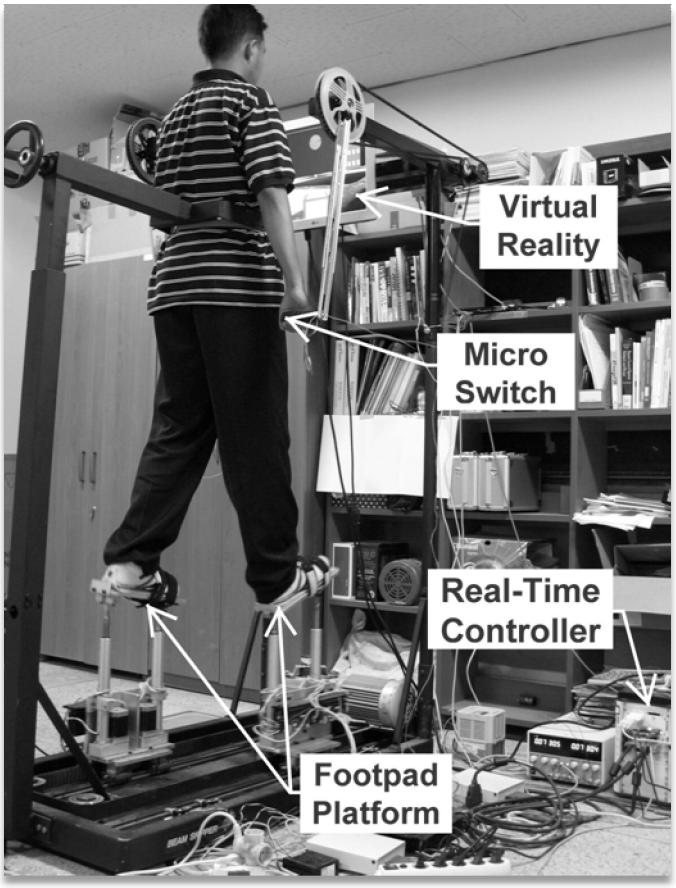

Figure 6-1 Experiment with a healthy subject

6.2 Results

Figures of sequences of snapshots of walking on level ground, walking up stairs and walking up slope are shown in Appendix C. Figure 6-2 shows the actual response of the slider and the upper limb motions. The upper limb output is disturbed by the subject, since the subject is trying to change the walking velocity. In Figure 6-3,

the velocity profiles of the slider and the upper limb are showing that the velocity is increasing and decreasing gradually. The walking velocity changes from the initial 0.05 m/s to 0.1 m/s and then back to the initial value. The $T_{d,est}$ is shown in Figure 6-4. When the absolute of $T_{d,est}$ is above the threshold value, the period of positive or negative signal is accumulated, then at the next stride the velocity is updated proportional to accumulated period. For this case, the toe and heel trajectories of the right foot are shown in Figure 6-5.

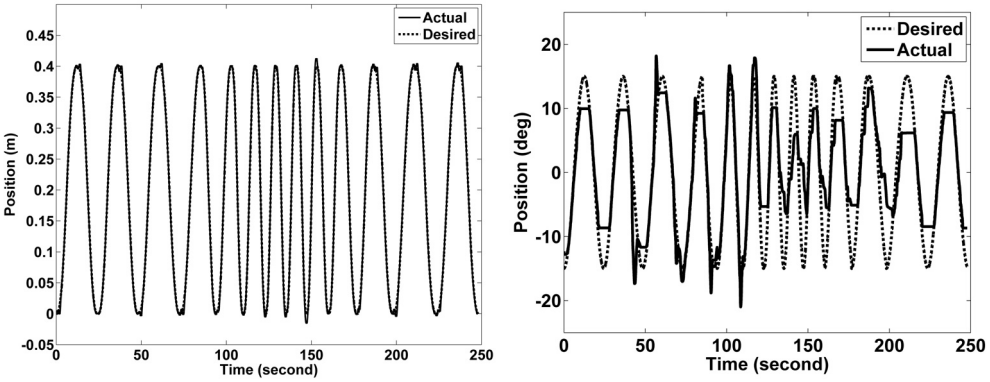

Figure 6-2 Desired Vs actual positions of the slider (left) and the upper limb (right)

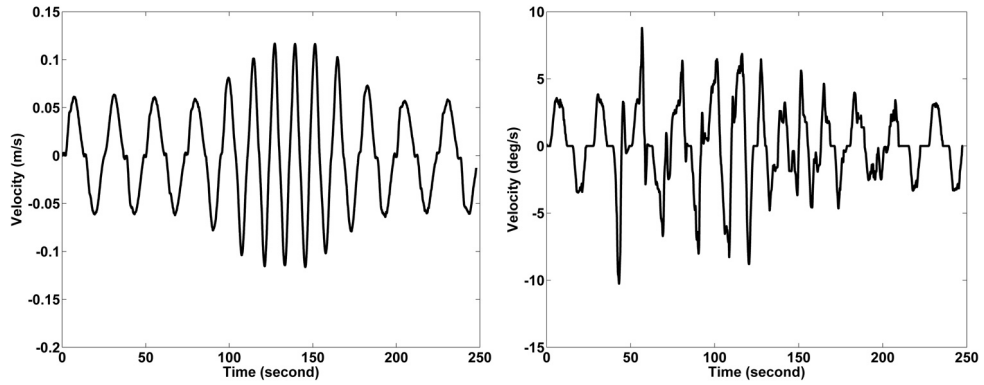

Figure 6-3 Velocity profile of the slider (left) and the upper limb (right)

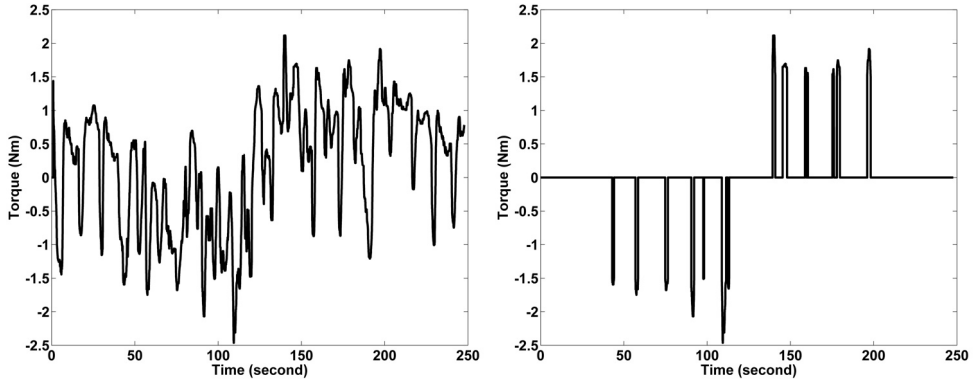

Figure 6-4 Estimated disturbance torque (left), and with threshold 1.5 Nm (right)

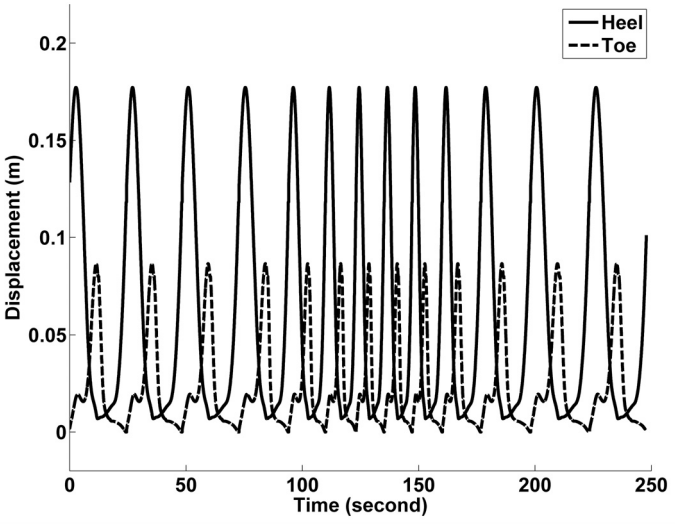

Figure 6-5 The trajectory profile of toe and heel during level walking

Another two trials with stairs and slope for walking on various terrain types have been done. The step length for walking up stairs and slope are 0.3 meter and 0.4 meter respectively. Figure 6-6 and Figure 6-7 show the toe and heel trajectories, the lower limb velocities and the estimated torques over threshold during walking on stairs and slope respectively. These figures clearly show that the walking velocity on stairs and slope can also be updated through upper- and lower-limb connections and walking pattern synchronization.

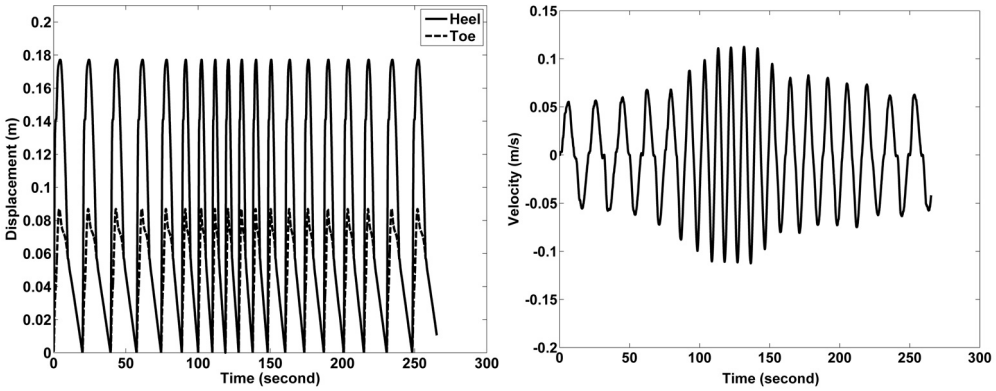

(a) **(b)**

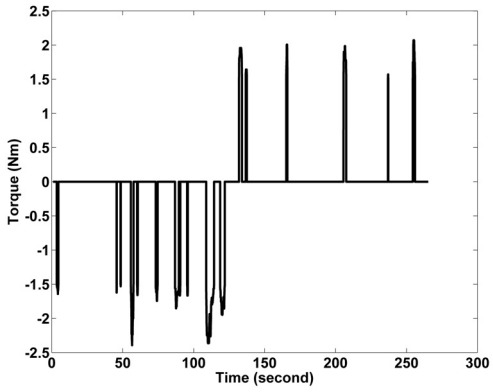

(c)

Figure 6-6 The trajectory profile of toe and heel during walking up stairs (a), the walking velocity (b), and estimated torque over threshold (c)

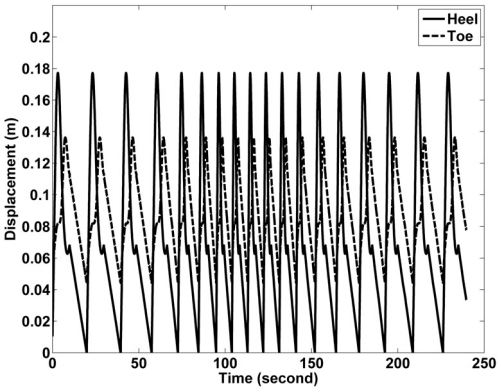

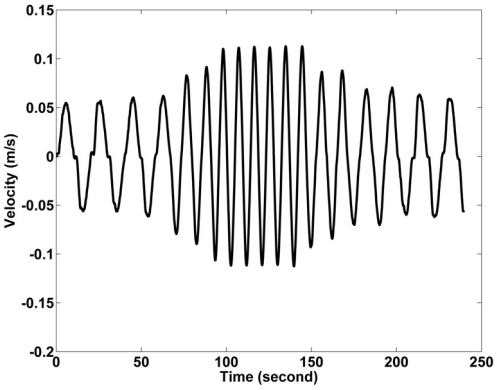

(a) **(b)**

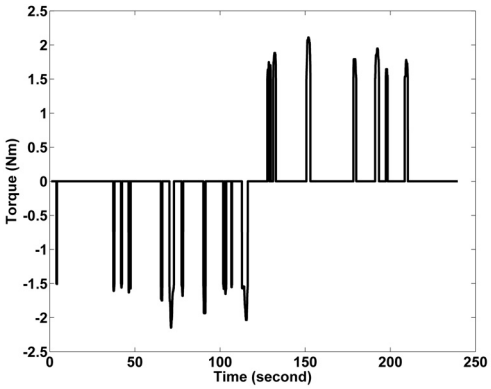

(c)

Figure 6-7 The trajectory profile of toe and heel during walking up slope (a), the walking velocity (b), and estimated torque over threshold (c)

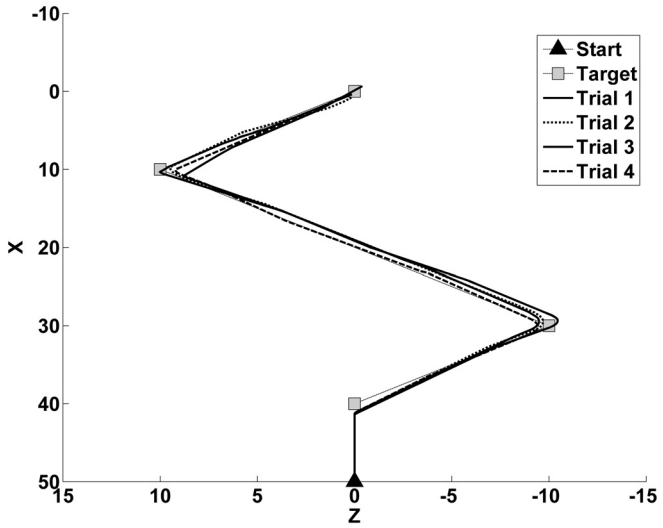

Figure 6-8 The position of the user in virtual environment

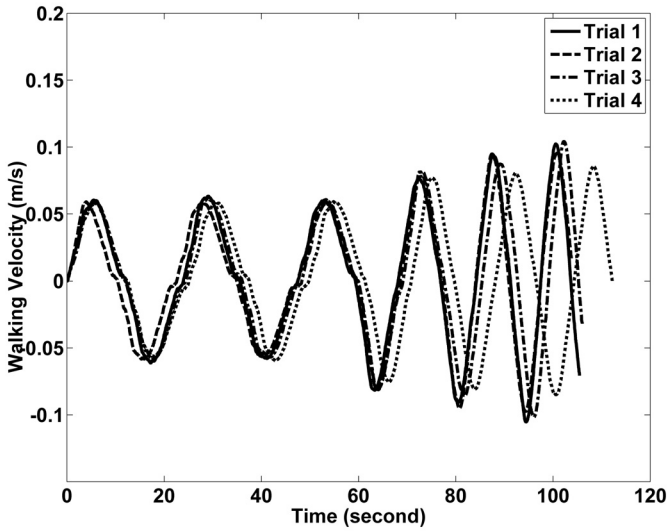

Figure 6-9 Walking velocity plots of the 4 trials during navigation

Four navigation trials in the VE were conducted. The subject was asked to approach the four target boxes in a zigzag path. When walking, he was also asked to change the walking velocity by manipulating the swing motion of the robot arm. The initial walking velocity is 0.05 m/s and with maximum 0.1 m/s. Figure 6-8 shows the positions of the targets and the subject in the VE environment; the subject was able to carry out the given task. Figure 6-9 shows the walking velocity during navigation in VE. The walking velocities when the subject reached the last target are varying since that depends on the subject's intentions. From the figures, it is shown that the subject was able to change his walking velocity and navigate in VE until he reached the final target.

Chapter 7

7 Conclusions and Discussions

We described a 6-DOF gait rehabilitation robot with upper- and lower limb connections. Adequate upper- and lower-limb connections during walking could be achieved through the mechanical design, a synchronized walking pattern and an interaction control for walking velocity update. Several contributions of this work are:

- The design of the gait rehabilitation robot which considers the upper limb effect on human gait rehabilitation is novel
- The robot has small power consumption, compact design which allows the gait rehabilitation at home compared to the existing programmable footplate-type robot
- The algorithm proposed to update the walking velocity by upper limb and lower limb interactions is new (esp. in programmable footplate type gait rehab. approach)
- The navigation in VE combining the upper limb and walking velocity update -to best of our knowledge- is also new

Walking experiments with a healthy subject on level walking, stairs and slope have been done for applying walking velocity update even on various terrain types. Results show that through the interaction between the human and robot arms, the subject is able to successfully update his walking velocity. Moreover, a VR navigation

experiment in which the subject was asked to accomplish a certain task has been conducted. The result shows that the walking velocity profile can be updated during the navigation in VEs. Through this development, training modes of gait rehabilitation can be more effectively combined to VEs and can allow more choices for upper limb coordination.

Currently, the body weight support system (BWS) and the foot measurement system are being manufactured and could not be presented in this thesis. However, after the manufacturing is finished and the experiments have been conducted, the results shall be published accordingly. For future work, we will study the kinematics of upper limb motions during stepping on various terrain types, develop navigation algorithms for vertical motions, and perform clinical tests with the prototype of the gait rehabilitation robot.

Appendix A

Controller Derivations

a. AC servo motor control (base slider)

The difference between AC Servo Motor and DC servo motor is the design of the motor where in AC servo motor the permanent magnet is on the rotor. The block diagram of an AC servo motor is very similar to the block diagram of DC servo motor.

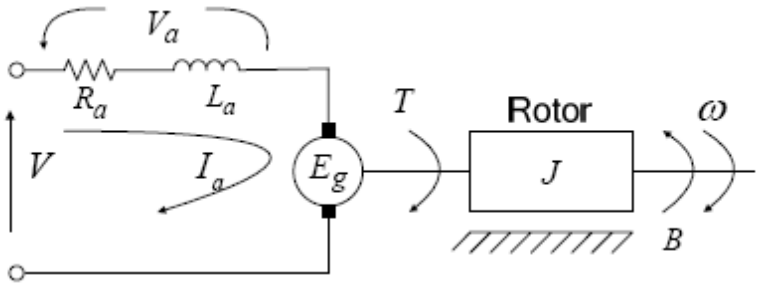

Figure A-1 Schematic of a DC motor, Va is armature voltage, Ia is armature current, Ra is armature resistance, La is armature inductance, V is voltage input, J is motor inertia, B is motor damping, T_m is motor torque, ω is motor shaft angular velocity, θ is motor shaft angle and T_d is external disturbance

From Figure A-1:

$$I_a R_a + L_a \frac{dI}{dt} + K_b \frac{d\theta}{dt} = V \tag{A.1}$$

$$T - T_{LOAD} = K_t \; I_{a-} \; T_{LOAD} = T_j + T_b$$

$$= J \frac{d^2\theta}{dt^2} + B \frac{d\theta}{dt} \tag{A.2}$$

$$I_a = \frac{1}{K_t}\left(J \frac{d^2\theta}{dt^2} + B \frac{d\theta}{dt}\right) + T_{LOAD} \tag{A.3}$$

Substituting (A.3) → (A.1):

$$V = \frac{R_a}{K_t}\left(J \frac{d^2\theta}{dt^2} + B \frac{d\theta}{dt} + T_{LOAD}\right) + \frac{L_a}{K_t}\frac{d}{dt}\left(J \frac{d^2\theta}{dt^2} + B \frac{d\theta}{dt} + T_{LOAD}\right)$$

$$+K_b \frac{d\theta}{dt}$$

$$= \frac{JR_a}{K_t}\frac{d^2\theta}{dt^2} + \frac{BR_a}{K_t}\frac{d\theta}{dt} + \frac{R_a}{K_t}T_{LOAD} + \frac{JL_a}{K_t}\frac{d^3\theta}{dt^3} + \frac{BL_a}{K_t}\frac{d^2\theta}{dt^2} + \frac{L_a}{K_t}T'_{LOAD}$$

$$+K_b \frac{d\theta}{dt} \tag{A.4}$$

We obtain:

$$\dot{\theta}_{1=}\theta_2$$

$$\dot{\theta}_{2=}\theta_3$$

$$\dot{\theta}_3 = \frac{K_t}{JL_a}V - \frac{B}{J}\theta_3 - \frac{R_a}{L_a}\theta_3 - \frac{R_aB}{JL_a}\theta_2 - \frac{K_bK_t}{JL_a}\theta_2 - \frac{L_a}{JK_t}T'_{LOAD}$$

$$-\frac{R_a}{L_aJ}T_{LOAD} \qquad \text{(A.5)}$$

Having 3rd order system:

$s = \left(\frac{d}{dt} + \lambda\right)^{r-1}\tilde{\theta}$, where $r = 3$ and $\tilde{\theta} = \theta - \theta_d$

$$= \left(\frac{d}{dt} + \lambda\right)^2 \tilde{\theta}$$

$$= \frac{d^2\tilde{\theta}}{dt^2} + 2\lambda\frac{d\tilde{\theta}}{dt} + \lambda^2\tilde{\theta}$$

$$= \ddot{\tilde{\theta}} + 2\lambda\dot{\tilde{\theta}} + \lambda^2\tilde{\theta}$$

$$= \left(\ddot{\theta} - \ddot{\theta}_d\right) + 2\lambda\left(\dot{\theta} - \dot{\theta}_d\right) + \lambda^2(\theta - \theta_d) \qquad \text{(A.6)}$$

We try to force the state trajectory to slide on our surface so that:

$s = 0$

$\dot{s} = 0$

Therefore,

$$\dot{s} = \left(\dddot{\theta} - \dddot{\theta}_d\right) + 2\lambda\left(\ddot{\theta} - \ddot{\theta}_d\right) + \lambda^2\left(\dot{\theta} - \dot{\theta}_d\right) \qquad \text{(A.7)}$$

$$0 = \frac{K_t}{JL_a}V - \frac{B}{J}\theta_3 - \frac{R_a}{L_a}\theta_3 - \frac{R_aB}{JL_a}\theta_2 - \frac{K_bK_t}{JL_a}\theta_2 - \frac{L_a}{JK_t}T'_{LOAD}$$

$$-\frac{R_a}{JL_a}T_{LOAD} - \ddot{\theta}_d + 2\lambda\left(\theta_3 - \ddot{\theta}_d\right) + \lambda^2\left(\theta_2 - \dot{\theta}_d\right)$$

Obtaining the equivalent control:

$$V_{eq} = \frac{BL_a}{K_t}\theta_3 + \frac{L_a}{K_t}T'_{LOAD} + \frac{JR_a}{K_t}\theta_3 + \frac{BR_a}{K_t}\theta_2 + \frac{R_a}{K_t}T_{LOAD} + K_b\theta_2 + \frac{JL_a}{K_t}\ddot{\theta}_d - 2\lambda\frac{JL_a}{K_t}(\theta_3 - \ddot{\theta}_d) - \lambda^2\frac{JL_a}{K_t}(\theta_2 - \dot{\theta}_d) \quad \text{(A.8)}$$

Then, the SMC controller:

$$V = V_{smc} = V_{eq} + V_{switching}, \text{ where } V_{switching} = -Ksat\left(\frac{s}{\phi_u}\right) \quad \text{(A.9)}$$

where sat is the function of:

$sign(s)$, If $abs(s) > \phi_u$

$\frac{s}{\phi_u}$, If $abs(s) < \phi_u$

Thus, the complete controller is obtained as:

$$\begin{aligned} V_{smc} &= V_{eq} + V_{switching} \\ &= \frac{BL_a}{K_t}\theta_3 + \frac{L_a}{K_t}T'_{LOAD} + \frac{JR_a}{K_t}\theta_3 + \frac{BR_a}{K_t}\theta_2 \\ &\quad + \frac{R_a}{K_t}T_{LOAD} + K_b\theta_2 + \frac{JL_a}{K_t}\ddot{\theta}_d - 2\lambda\frac{JL_a}{K_t}(\theta_3 - \ddot{\theta}_d) \\ &\quad - \lambda^2\frac{JL_a}{K_t}(\theta_2 - \dot{\theta}_d) - Ksat\left(\frac{s}{\phi_u}\right) \end{aligned} \quad \text{(A.10)}$$

Proof of stability

We ensure the stability of our system choosing K to be large enough so that stable in the sense of Lyapunov.

We introduce Lyapunov candidate:

$$V = \frac{1}{2}s^2 \succ 0 \tag{A.11}$$

Then,

$$\dot{V} = s\dot{s} = s(\frac{K_t}{JL_a}V - \frac{B}{J}\theta_3 - \frac{R_a}{L_a}\theta_3 - \frac{BR_a}{JL_a}\theta_2 - \frac{K_bK_t}{JK_t}\theta_2 - \frac{L_a}{JK_t}T'_{LOAD}$$
$$-\frac{R_a}{L_aJ}T_{LOAD} - \ddot{\theta}_d + 2\lambda(\theta_3 - \ddot{\theta}_d) + \lambda^2(\theta_2 - \dot{\theta}_d) - Ksat(\frac{s}{\phi_u}))$$
$$= s(f - Ksat(\frac{s}{\phi_u}))$$

Thus by choosing K large enough, we can guarantee that:

$$sf - K|s| \leq 0$$

which fulfill the Lyapunov stability condition.

b. BLDC motor control (upper limb)

SMC is one of the robust controllers with ability to compensate the uncertain parameters, incomplete dynamics model and reject disturbances. The additional of PI on the SMC give several “extra” freedoms and flexibility in tuning and obtaining the desired performance.

First, select a PI sliding surface. Second, from the sliding surface we derive the equivalent control. Third, the control output is achieved by adding the switching control output.

The dynamics of a DC motor is known as:

$$J\ddot{\theta} + B\dot{\theta} = T_m + T_d \tag{A.13}$$

Where:

J is motor inertia

B is motor damping

T_m is motor torque

T_d is disturbance

A PI sliding surface is defined as:

$$S = K_p\breve{\theta} + K_i\int_0^t \breve{\theta}\, dt + \dot{\breve{\theta}}, \text{ where } \breve{\theta} = \theta - \theta_d \tag{A.14}$$

We try to force the state trajectory to slide on our surface so that:

$s = 0$

$\dot{s} = 0$

Thus,

$$\begin{aligned}\dot{S} &= K_p\ddot{\breve{\theta}} + K_i\dot{\breve{\theta}} + \dddot{\breve{\theta}} \\ &= K_p\left(\dot{\theta}_m - \dot{\theta}_d\right) + K_i\left(\theta_m - \theta_d\right) + \left(\ddot{\theta}_m - \ddot{\theta}_d\right)\end{aligned}$$

$$= K_p\left(\dot{\theta}_m - \dot{\theta}_d\right) + K_i\left(\theta_m - \theta_d\right) + \frac{T_m}{J} - \frac{B}{J}\dot{\theta}_m - \ddot{\theta}_d = 0 \qquad \text{(A.15)}$$

Since $T_m = K_t I_a$, where K_t is motor constant, I_a is armature current, then the equivalent control is obtained as:

$$I_{eq} = \left(-JK_{p(\dot{\theta}_m - \dot{\theta}_d)} - JK_i(\theta_m - \theta_d) + B\dot{\theta}_m\right)/K_t \qquad \text{(A.16)}$$

The complete controller is obtained as:

$$I = I_{pismc} = I_{eq} + I_{switching}, \text{ where } I_{switching} = -n\, sat(\frac{s}{\phi_l})$$

$$= \left(\left(-JK_{p(\dot{\theta}_m - \dot{\theta}_d)} - JK_i(\theta_m - \theta_d) + B\dot{\theta}_m\right)/K_t\right) - n\, sat(\frac{s}{\phi_l}) \qquad \text{(A.17)}$$

where sat is the function of:

$sign(s)$, If $abs(s) > \phi_l$

$\frac{s}{\phi_l}$, If $abs(s) < \phi_l$

Proof of stability

We ensure the stability of our system choosing K to be large enough so that stable in the sense of Lyapunov.

We introduce Lyapunov candidate:

$$I = \frac{1}{2}s^2 \succ 0 \qquad \text{(A.18)}$$

Then,

$$\dot{I} = s\dot{s} = s(K_p(\dot{\theta}_m - \dot{\theta}_d) + K_i\,(\theta_m - \theta_d) + \frac{T_m}{J} - \frac{B}{J}\dot{\theta}_m - \ddot{\theta}_d$$

$$- n\,sat(\frac{s}{\phi_l}))$$

$$= s(f - n\,sat(\frac{s}{\phi_l})) \qquad \text{(A.19)}$$

Thus by choosing n large enough, we can guarantee that:

$$sf - n\,|s\,| \leq 0$$

which fulfill the Lyapunov stability condition.

Appendix B

Graphical User Interface

a. Control Program

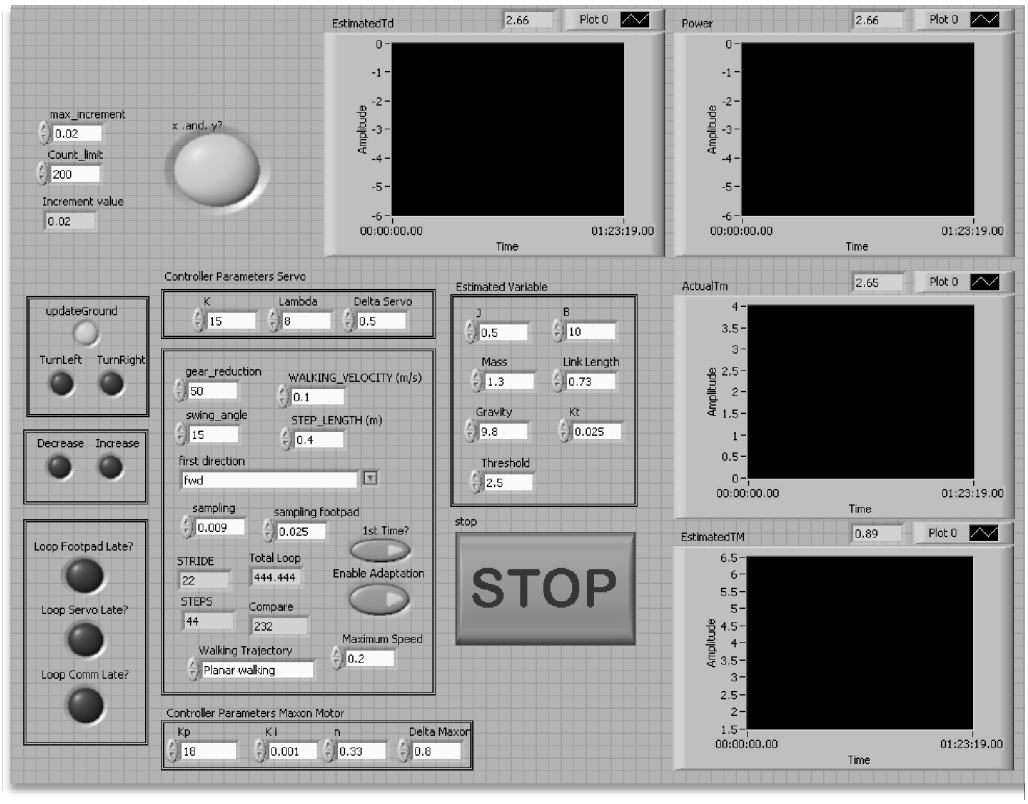

Figure B-1 GUI of the main program (beta)

b. Program Flowchart

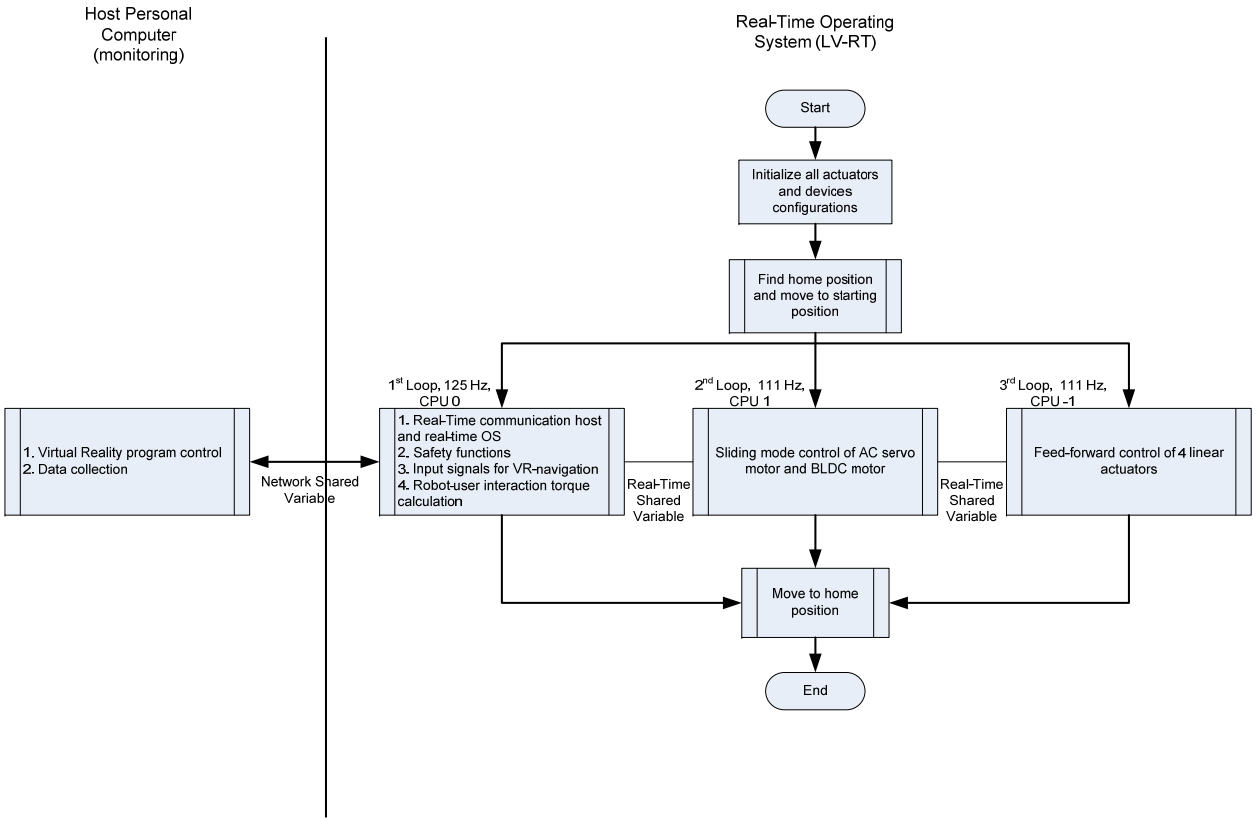

Figure B-2 High-level flowchart of the main program

Appendix C

Figures of Snapshots

Figure C-1 Sequence of successive snapshots showing a stride of level walking

Figure C-2 Sequence of successive snapshots showing the up-stairs walking

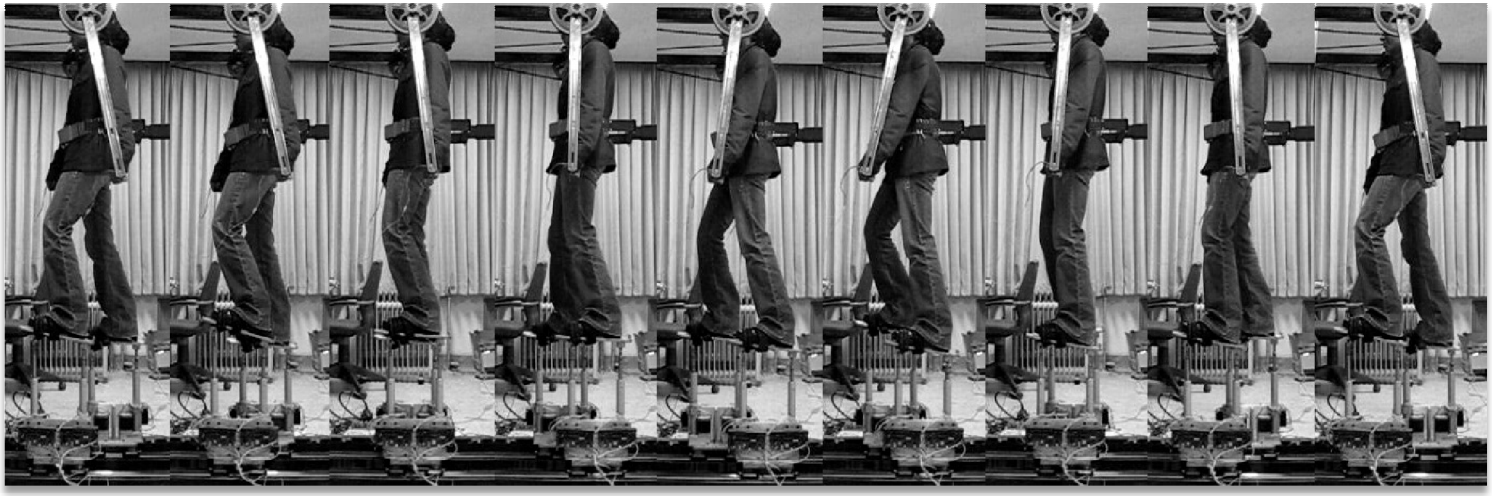

Figure C-3 Sequence of successive snapshots showing the up-slope walking

Bibliography

[1] J. Perry, *Gait Analysis: Normal and Pathological Function*. Thorofare, NJ: Slack Inc., 1992.

[2] J. F. Veneman, *Design and Evaluation of The Gait Rehabilitation Robot LOPES, PhD Thesis*. Enschede, The Netherlands: University of Twente, 2007.

[3] S. J. Cuccurullo, *Physical medicine and rehabilitation board review*, S. J. Cuccurullo, Ed. New York, United States of America: Demos Medical Publishing, 2004.

[4] S. J. Olney and C. Richards, "Hemiparetic Gait Following Stroke. Part I: Characteristics," *Gait and Posture*, vol. 4, no. 2, pp. 136-148, Nov. 2996.

[5] J. W. Wheeler, *An Ankel Robot for a Modular Gait Rehabilitation System, Master Thesis*. Massachusetts Institute of Technology, 2004.

[6] K. Gert, K. Boudewijn, and L. Eline, "Understanding the pattern of functional recovery after stroke: Facts and theories," *Restorative Neurology and Neuroscience*, vol. 22, pp. 281-299, 2004.

[7] B. B. Johansson, "Brain Plasticity and Stroke Rehabilitation: The Willis Lecture," *Stroke*, vol. 31, pp. 223-230, 2000.

[8] M. C. Cirstea and M. F. Levin, "Compensatory strategies for reaching in stroke," *Brain*, vol. 123, pp. 940-953, 2000.

[9] I. H. Robertson and J. M. J. Murre, "Rehabilitation of Brain Damage: Brain Plasticity and Principles of Guided Recovery," *Psychological Bulletin*, vol. 125, no. 5, pp. 544-575, 1999.

[10] S. Hesse, C. Bertelt, A. Schaffrin, and K. H. Mauritz, "Restoration of gait in non-ambulatory hemiparetic patients by treadmill training with partial body weight support," *Arch. Phys. Med. Rehabil.*, vol. 75, no. 10, pp. 87-1093, Oct. 1994.

[11] B. H. Dobkin, "An Overview of Treadmill Locomotor Training with Partial Body Weight Support: A Neurophysiologically Sound Approach Whose Time Has Come for Randomized Clinical Trials," *Neurorehabilitation and Neural Repair*, vol. 13, no. 3, pp. 157-165, 1999.

[12] C. Werner, S. v. Frankenberg, T. Treig, M. Konrad, and S. Hesse, "Treadmill Training With Partial Body Weight Support and an Electromechanical Gait Trainer for Restoration of Gait in Subacute Stroke Patients: A Randomized Crossover Study," *Stroke*, vol. 33, 2002.

[13] G. Colombo, M. Wirz, and V. Dietz, "Driven gait orthosis for improvement of locomotor training in paraplegic patients," *Spinal Cord*, vol. 39, no. 5, pp. 252-255, May 2001.

[14] S. Hesse and D. Uhlenbrock, "A mechanized gait trainer for restoration of gait," *Journal of rehabilitation research and*

development, vol. 37, no. 6, pp. 701-708, 2000.

[15] S. Jezernik, G. Colombo, and M. Morari, "Automatic Gait-Pattern Adaptation Algorithms for Rehabilitation With a 4-DOF Robotic Orthosis," *IEEE Trans. on Robotics and Automation*, vol. 20, no. 3, pp. 574-582, 2004.

[16] H. Schmidt, S. Hesse, R. Bernhardt, and J. Krüger, "HapticWalker-A Novel Haptic Foot Device," *ACM Transactions on Applied Perception*, vol. 2, no. 2, pp. 166-180, Apr. 2005.

[17] S. Freivogel, J. Mehrholz, T. Husak-Sotomayor, and D. Schmalohr, "Gait training with the newly developed 'LokoHelp'-system is feasible for nonambulatory patients after stroke, spinal cord and brain injury. A feasibility study," *Brain Injury*, vol. 22, no. 7, pp. 625-632, 2008.

[18] J. F. Veneman, et al., "Design and Evaluation of the LOPES Exoskeleton Robot for Interactive Gait Rehabilitation," *IEEE Transactions on Neural Systems and Rehabilitation Engineering*, vol. 15, no. 3, pp. 379-386, 2007.

[19] D. J. Reinkensmeyer, et al., "Tools for understanding and optimizing robotic gait training," *Journal of Rehabilitation Research & Development*, vol. 43, no. 5, pp. 657-670, 2006.

[20] J. von Zitzewitz, M. Bernhardt, and R. Riener, "A Novel Method for Automatic Treadmill Speed Adaptation," *IEEE Transactions on Neural Systems and Rehabilitation Engineering*, vol. 15, no. 3, pp. 401-409, 2007.

[21] S. K. Banala, et al., "Gravity-Balancing Leg Orthosis and Its Performance Evaluation," *IEEE Transactions on Robotics*, vol. 22, no. 6, pp. 1228-1239, Dec. 2006.

[22] H. Yano, K. Kasai, H. Saitou, and H. Iwata, "Development of a Gait Rehabilitation System Using a Locomotion Interface," *The Journal of Visualization and Computer Animation*, vol. 14, no. 5, pp. 243-252, Nov. 2003.

[23] M. Holden, E. Todorov, J. Callahan, and e. al., "Virtual Environment Training Improves Motor Performance in Two Patients with Stroke: Case Report," *Neurology Report*, vol. 23, pp. 57-67, 1999.

[24] (2008, Jul.) VR in Gait Rehab. [Online]. HYPERLINK "http://www.cs.odu.edu/~jrcrouch/nigel/VRGaitRehab.html" http://www.cs.odu.edu/~jrcrouch/nigel/VRGaitRehab.html

[25] R. Boian, *Robotic Mobility Rehabilitation System Using Virtual Reality, PhD Thesis*. Rutgers University, ECE Dept., January 2005.

[26] D. L. Jaffe, D. A. Brown, C. D. Pierson-Carey, and e. al., "Stepping Over Obstacles to Improve Walking in Individuals with Post-Stroke Hemiplegia," *Journal of Rehabilitation Research and Development*, vol. 41, pp. 283-292, 2004.

[27] M. Wellner, et al., "Obstacle Crossing in a Virtual Environment with the Rehabilitation Gait Robot Lokomat, J. D. Westwood et al. (Eds.)," *Medicine meets virtual reality*, vol. 15, pp. 497-499,

2007.

[28] J. Yoon and J. Ryu, "A Novel Locomotion Interface with Two 6-DOF Parallel Manipulators That Allows Human Walking on Various Terrains," *International Journal of Robotics Researches*, vol. 25, no. 7, pp. 689-708, Jul. 2006.

[29] R. P. Darken, W. R. Cockayne, and D. Carmein, "The omni-directional treadmill: a locomotion device for virtual worlds," in *User Interface Software Technology*, 1997, pp. 213-222.

[30] H. Iwata, "The Torus Treadmill: Realizing Locomotion in VEs," *IEEE Computer Graphics and Applications*, vol. 19, no. 6, pp. 30-35, 1999.

[31] R. N. Hinrichs, "Whole body movement: coordination of arms and legs in walking and running," in *J. M. Winters and S. L. Y. Woo*. New York: Springer-Verlag, 1990, pp. 694-705.

[32] T. Wannier, C. Bastiaanse, G. Colombo, and V. Dietz, "Arm to leg coordination in humans during walking, creeping and swimming activities," *Experimental Brain Research*, vol. 141, no. 2, pp. 375-379, Sep. 2001.

[33] D. P. Ferris, H. J. Huang, and P.-C. Kao, "Moving The Arms To Activate The Legs," *Exercise and Sport Sciences Reviews*, vol. 34, no. 3, pp. 113-120, Jul. 2006.

[34] H. Elftman, *Human Biology*, 11th ed.. 1939.

[35] V. Dietz, K. Fouad, and C. M. Bastiaanse, "Neuronal coordination of arm and leg movements during human locomotion," *European*

Journal of Neuroscience, vol. 14, pp. 1906-1914, 2001.

[36] H. J. Huang and D. P. Ferris, "Neural coupling between upper and lower limbs during recumbent stepping ," *Journal of Applied Physiology*, vol. 97, pp. 1299-1308, Jun. 2004.

[37] P. C. Kao and D. P. Ferris, "The Effect of Movement Frequency on Interlimb Coupling During Recumbent Stepping," *Motor Control*, vol. 9, pp. 144-163, 2005.

[38] J. Yoon, J. Ryu, and K. Lim, "A Novel Reconfigurable Ankle Rehabilitation Robot for Various Exercise Modes," *Journal of Robotic Systems*, vol. 22, no. 1, pp. 15-33, 2006.

[39] D. A. Lawrence, "Impedance Control Stability Properties in Common Implementations," in *IEEE International Conference on Robotics and Automation*, Philadelphia, 1988, pp. 1185-1190.

[40] A. L. Behrman and S. J. Harkema., "Locomotor training after human spinal cord injury: a series of case studies," *Physical Therapy*, vol. 80, pp. 688-700, 2000.

[41] V. G. Popescu, G. C. Burdea, M. Bouzit, and V. R. Hentz, "A Virtual-Reality-Based Telerehabilitation System with Force Feedback," *IEEE Transactions on Information in Biomedicine*, vol. 4, no. 1, pp. 45-51, Mar. 2000.

[42] J. Yoon, J. Park, Y. Lim, and J. Ryu, "A Planar Symmetric Walking Cancellation Algorithm for a Foot-Platform Locomotion Interface," *International Journal of Robotics Researches (Conditionally Accepted)*, 2008.

[43] R. C. Wagenaar and R. E. A. van Emmerik, "Resonant frequencies of arms and legs identify different walking patterns," *Journal of Biomechanics*, vol. 33, no. 7, pp. 853-861, Jul. 2000.

[44] M. Kubo, R. C. Wagenaar, E. Saltzman, and K. G. Holt, "Biomechanical mechanism for transitions in phase and frequency of arm and leg during walking," *Biological Cybernetics*, vol. 91, pp. 91-98, 2004.

[45] B. Novandy, Christiand, and J. Yoon, "The Development of Gait Rehabilitation Robot Driven by Upper Limb Motion," in *International Conference on Control, Automation and Systems*, 2007, pp. 2383-2388.

[46] J. Yoon and J. Ryu, "The Development of the 3-DOF Planar Parallel Robot (RRR Type) for Omni-directional Locomotion Interface," in *3rd IFAC Symposium on Mechatronic Systems*, 2004, pp. 66-72.

[47] J. J. E. Slotine and W. Li, *Applied Nonlinear Control*, 1st ed.. New Jersey: Prentice-Hall, 1991.

[48] M. W. Spong, S. H., and M. Vidyasagar, *Robot Modeling and Control*. Joh Wiley and Sons, 2006.

[49] D. A. Winter, "Foot trajectory in human gait: a precise and multifactorial motor control task ," *Physical Therapy*, vol. 72, no. 1, pp. 45-53, Jan. 1992.

[50] B. H. Dobkin, *The Clinical Science of Neurologic Rehabilitation*,

2nd ed.. Oxford University Press, 2003.

[51] P. W. Duncan, "Stroke Disability," *Physical Therapy*, vol. 74, no. 5, pp. 399-407, May 1994.

Acknowledgments

This thesis was carried out under the direction of Professor Yoon Jungwon, Department of Mechanical and Aerospace Engineering, Gyeongsang National University. This work was supported by the Korea Research Foundation Grant funded by the Korean Government (MOEHRD)(KRF-2006-331-D00022) and was supported by 2nd stage BK21 Project.

I would like to thank Allah Azza wa Jalla for everything He has given me, and for His guidance to the Sunnah. If not by His mercy, I am surely will not be able to become what I am now. My sincere gratitude goes to Prof. Jungwon Yoon, PhD for his advice and mentor throughout my two years. I would like to thank him for this opportunity to join his lab to pursue my Master degree. I would also like to thank Dr. Gandjar Kiswanto for helping me with the applications and persuasion in pursuing higher degree; he was my advisor during my tremendous moments in Robotics Team University of Indonesia. I would like to thank Dr. Prasanth Kumar who has been helping me a lot with valuable discussions. To Nandha and Christiand, both had been helping me many times during my first year in Korea. Last but not least, I would like to show my deep gratitude to my parents and my family, for their love, support and prayer. Hopefully with the knowledge that I have learned here would be beneficial to myself, my family and humanity, insyaAllah.